Journal of Medicinal Chemistry

Article

Cite This: J. Med. Chem. 2019, 62, 9560−9575

pubs.acs.org/jmc

Metallacarborane Sulfamides: Unconventional, Specific, and Highly Selective Inhibitors of Carbonic Anhydrase IX

Bohumír Grüner,[*,†,○] Jiří Brynda,[‡,§,○] Viswanath Das,[∥,#,○] Václav Šícha,[†,○] Jana Štěpánková,[∥,#] Jan Nekvinda,[†,▽] Josef Holub,[†] Klára Pospíšilová,[‡] Milan Fábry,[§] Petr Pachl,[‡] Vlastimil Král,[§] Michael Kugler,[‡] Vlastimil Mašek,[∥] Martina Medvedíková,[∥] Stanislava Matějková,[‡] Alice Nová,[∥] Barbora Lišková,[∥] Soňa Gurská,[∥] Petr Džubák,[∥,#] Marián Hajdúch,[*,∥,#,○] and Pavlína Řezáčová[*,‡,§,○]

[†]Institute of Inorganic Chemistry of the Czech Academy of Sciences, 250 68 Řež, Czech Republic

[‡]Institute of Organic Chemistry and Biochemistry of the Czech Academy of Sciences, Flemingovo nám. 2, 16610 Prague, Czech Republic

[§]Institute of Molecular Genetics of the Czech Academy of Sciences, Flemingovo nam. 2, 16610 Prague, Czech Republic

[∥]Institute of Molecular and Translational Medicine, Olomouc, Hněvotínská 1333/5, 77900 Olomouc, Czech Republic

[#]Cancer Research Czech Republic, Hněvotínská 5, 77900 Olomouc, Czech Republic

[▽]Department of Organic Chemistry, Faculty of Natural Science, Charles University, Hlavova 2030, 12800 Prague 2, Czech Republic

Supporting Information

ABSTRACT: Carbonic anhydrase IX (CAIX) is a transmembrane enzyme that regulates pH in hypoxic tumors and promotes tumor cell survival. Its expression is associated with the occurrence of metastases and poor prognosis. Here, we present nine derivatives of the cobalt bis(dicarbollide)(1−) anion substituted at the boron or carbon sites by alkysulfamide group(s) as highly specific and selective inhibitors of CAIX. Interactions of these compounds with the active site of CAIX were explored on the atomic level using protein crystallography. Two selected derivatives display subnanomolar or picomolar inhibition constants and high selectivity for the tumor-specific CAIX over cytosolic isoform CAII. Both derivatives had a time-dependent effect on the growth of multicellular spheroids of HT-29 and HCT116 colorectal cancer cells, facilitated penetration and/or accumulation of doxorubicin into spheroids, and displayed low toxicity and showed promising pharmacokinetics and a significant inhibitory effect on tumor growth in syngenic breast 4T1 and colorectal HT-29 cancer xenotransplants.

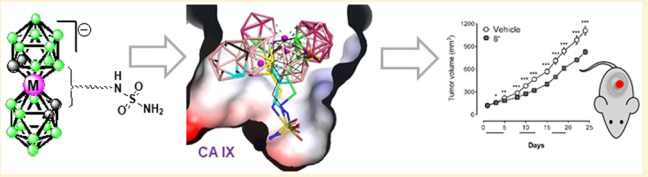

INTRODUCTION

Human carbonic anhydrases (CAs) are zinc metalloenzymes that catalyze the reversible hydration of carbon dioxide to bicarbonate and a proton, a reaction that is essential for many physiological processes. To date, 15 human CAs with different subcellular localizations and tissue expression profiles have been identified, and several isoforms are recognized as therapeutic targets for the treatment of various diseases.[1] The membrane-bound extracellular enzyme CAIX is highly expressed in the hypoxic regions of many solid tumors, while its expression in normal tissues is low or absent. It plays a critical role in tumor progression and is a validated target for cancer treatment.[1−4] Inhibition of CAIX has blocked tumor growth in multiple cancer models.[5]

Traditional CA inhibitors that have been used clinically for more than 50 years contain a sulfonamide or sulfamide moiety that coordinates the zinc cation in the CA catalytic site linked to an aryl ring either directly or via a linker.[6−10] CA isoforms share a high degree of sequence and structure similarity, especially in the active site,[11] and design of compounds with improved isoform selectivity is challenging.[12−14]

The isomeric 12-vertex dicarbaboranes (*ortho*-, *meta*- and *para*-$C_2B_{10}H_{12}$) and the 11-vertex *nido*-$[7,8\text{-}C_2B_9H_{12}]^-$ anion are emerging as three-dimensional pharmacophores, typically replacing aromatic rings.[15−20] Dicarbaboranes not only act as hydrophobic space-filling phenyl mimetic but are also able to increase the interaction energy, in vivo stability, and bioavailability of the known drugs.[20,21] Previously, we introduced 12-vertex icosahedral carborane and 11-vertex *nido*-dicarbollide scaffolds into structures of sulfamide-type compounds, resulting in inhibitory activity in the micromolar range and promising selectivity toward CAIX.[22] Structural information about the active-site binding mode of these carborane inhibitors determined by high-resolution X-ray diffraction studies[22,23] aided further inhibitor design, leading to the metallacarborane-containing compounds presented in this work.

Despite the successful exploitation of icosahedral dicarbaboranes in drug design, relatively little attention has been paid

Received: June 13, 2019
Published: September 30, 2019

DOI: 10.1021/acs.jmedchem.9b00945
J. Med. Chem. 2019, 62, 9560−9575

Scheme 1. Synthesis of CAIX Inhibitors Based on Derivatization of Cobalt Bis(dicarbollide) Ion with Alkylsulfamido Group[a]

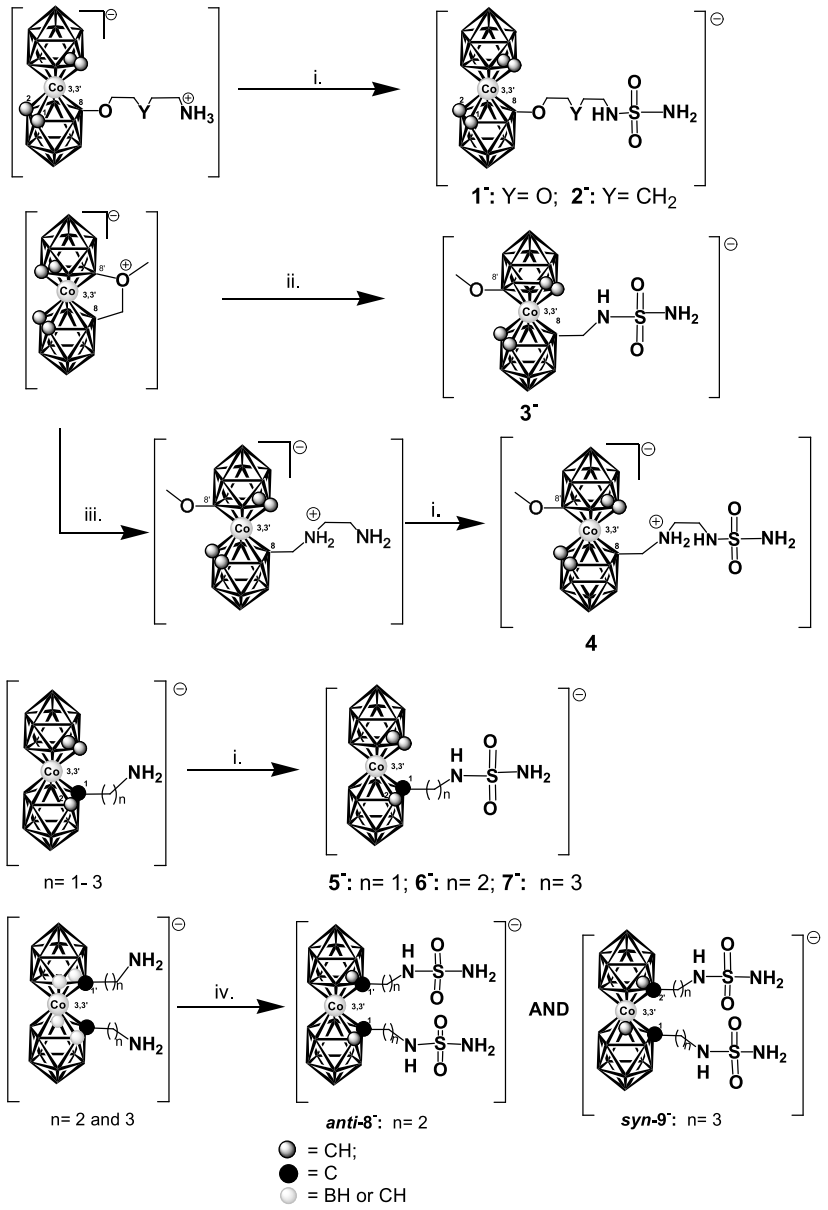

[a]Reagents and reaction conditions: (i) sulfamide (5 equiv), K_2CO_3, dioxane, reflux; (ii) sulfamide (5 equiv), DME, rt 7 days; (iii) NH_2-C_2H_4-NH_2, THF, rt, 30 min; (iv) sulfamide (10 equiv), K_2CO_3, dioxane, reflux.

to metallacarboranes and other chemically and thermally stable boron cage compounds.[18,20,24,25] Some smaller metallacarboranes have a cytostatic effect,[18,26−28] and derivatives of icosahedral cobalt bis(dicarbollide) ion $[(1,2\text{-}C_2B_9H_{11})_2\text{-}3,3'\text{-}Co]^-$ can specifically inhibit HIV protease.[29−32] Antiviral, antifungal, and antibacterial activity and the ability to penetrate artificial lipid bilayers and cellular membranes have been reported for some metallacarborane derivatives.[20,33−36]

Here, we report the synthesis and characterization of a series of sulfamide derivatives of the exceptionally stable cobalt bis(dicarbollide) ion. These compounds acted as highly potent and specific inhibitors of CAIX in vitro and in vivo. Crystal structures of the cobaltacarborane inhibitors bound to the CAIX active site confirmed that the enzyme cavity can easily accommodate the large cobalt bis(dicarbollide) cluster. Selected compounds exhibited a tumor-specific growth inhibitory effect in both two-dimensional (2D) and multicellular spheroid (MCS) cultures of CAIX-positive cell lines. Cellular distribution of the compounds was followed by Raman spectroscopy. Some compounds also showed favorable pharmacologic properties, as demonstrated using in vitro absorption, distribution, metabolism, and excretion (ADME) assays and in vivo pharmacokinetics methods. In mouse models, the compounds showed a significant anticancer effect in both syngenic breast (4T1-12B) and human xenografted HT-29 colorectal tumors.

RESULTS AND DISCUSSION

Design and Synthesis of Cobaltacarborate Sulfamides. In our previous work, we demonstrated that strongly hydrophobic icosahedral dicarbaborane cages along with *closo*-$[1\text{-}CB_{11}H_{12}]^-$ and *nido*-$[7,8\text{-}C_2B_9H_{12}]^-$ anions make promising inhibitors targeting the CAIX isoform when substituted with a zinc-coordinating sulfamide group.[22] On the basis of the crystal

DOI: 10.1021/acs.jmedchem.9b00945
J. Med. Chem. 2019, 62, 9560−9575

structure of carborane sulfamide bound to the enzyme active site and the fact that the highest CAIX selectivity was observed for the most sterically demanding ion, 7-propylsulfamido-8-phenyl-7,8-nido-undecaborate (K_i value of 2.7 μM and selectivity factor 18),[22] we hypothesized that increasing the size of the boron cluster would increase binding affinity and selectivity toward CAIX. We chose the cobalt bis(dicarbollide) ion to be evaluated as a hydrophobic, space-filling moiety to optimally fit the enzyme cavity. We also anticipated that ionic charge might contribute to increased affinity, as submillimolar inhibitory activity toward CAIX has been reported for simpler inorganic anions such as $S_2O_7^-$, RuO_4^-, ReO_4^-, $B_4O_7^-$, $[NbF_7]^-$, $[Ag(CN)_2]^-$, and $[Pd(CN)_4]^-$.[37]

The series of compounds presented here is based on cobalt bis(dicarbollide) ions substituted with a sulfamide group, which is accessible by transamination of amine or alkylamine precursors with inorganic sulfamide (see Scheme 1). We varied (i) the length of the linker between the sulfamide group and cluster, (ii) the site of substitution (at carbon or boron atoms), and (iii) the number of the groups attached to the cage. Fine-tuning of the structural motifs of boron-substituted compounds was limited by the availability of suitable synthetic substitution pathways. Compounds $\mathbf{1}^-$ and $\mathbf{2}^-$ were prepared from B(8)-substituted primary amines (Scheme 1). Those intermediates were obtained either by ring cleavage of the oxonium rings in $[(8\text{-}(O(CH_2CH_2)_2O)\text{-}1,2\text{-}C_2B_9H_{10})(1',2'\text{-}C_2B_9H_{11})\text{-}3,3'\text{-}Co]^0$ [38] or in the analogous pyrane derivative[39] using ammonia in THF (for details see Supporting Information and for an overview of these reagents and their reactions, see ref 40). This reaction sequence provided, after reaction with sulfamide, a six-atom-long heteroatom linker between the cobalt bis(dicarbollide) cluster and the terminal sulfamide group (Scheme 1).

Derivatives $\mathbf{3}^-$ and **4** were prepared by cleavage of the diatomic bridge present in $[(8,8'\text{-}\mu\text{-}CH_2O(CH_3)\text{-}(1,2\text{-}C_2B_9H_{10})_2\text{-}3,3'\text{-}Co]^0$ zwitterion[41] by a nitrogen nucleophile. Compound $\mathbf{3}^-$ was synthesized by direct cleavage of the bridge by sulfamide producing a methylene connector. This was followed by synthesis of **4**, in which the chain connecting the cage and head groups was elongated by additional three atoms. Compound **4** is zwitterionic due to protonation of the amine group present in the chain.

To explore further the effect of distance between the cage and sulfamide moiety and the differences in polar properties, we prepared alkylamino derivatives of the cobalt bis(dicarbollide) ion substituted at the cluster carbon atom.[42,43] The resulting compounds were subsequently converted to sulfamides of the general formulation $[(1\text{-}NH_2SO_2NH(CH_2)_n\text{-}1,2\text{-}C_2B_9H_{10})(1',2'\text{-}C_2B_9H_{11})\text{-}3,3'\text{-}Co]^-$ (n = 1−3), yielding $\mathbf{5}^-$ to $\mathbf{7}^-$. In addition to compounds with a single sulfamide group, we synthesized compounds containing two identical substituents at the cluster carbon atoms. In principle, substitutions at carbon atoms can lead to the presence of two or three diastereoisomers.[42,44] Only two sulfamide-substituted compounds could be isolated in the form of pure diastereoisomers: *anti*-$[1,1'\text{-}(NH_2SONHC_2H_4\text{-}1,2\text{-}C_2B_9H_{10})_2\text{-}3,3'\text{-}Co]^-$ ($\mathbf{8}^-$) and *syn*-$[1,2'\text{-}(NH_2SONHC_3H_6\text{-}1,2\text{-}C_2B_9H_{10})_2\text{-}3,3'\text{-}Co]^-$ ($\mathbf{9}^-$). The former substitution is asymmetric, corresponding to the racemic form; the latter corresponds to the *meso*-form. Isomers $\mathbf{8}^-$ and $\mathbf{9}^-$ were separated in the form of alkylhydroxy derivatives obtained after the initial step of the reaction sequence (for more details see Supporting Information and refs 42,43).

CAIX Inhibition in Vitro. CA inhibition was evaluated using an in vitro stopped-flow carbon dioxide hydration assay. To assess selectivity, inhibition of cancer-associated CAIX was compared with inhibition of the widespread CAII (Table 1).

Table 1. In Vitro Inhibition of Human CAII and CAIX Isoforms

compd	K_i (CAII) [nM]	K_i (CAIX) [nM]	selectivity index[a]
$\mathbf{1}^-$	156 ± 22	2.70 ± 0.46	57
$\mathbf{2}^-$	72 ± 10	0.98 ± 0.20	74
$\mathbf{3}^-$	466 ± 59	6.32 ± 1.20	74
4	510 ± 85	2.29 ± 0.29	222
$\mathbf{5}^-$	5.9 ± 1.2	0.12 ± 0.02	52
$\mathbf{6}^-$	26 ± 11	0.063 ± 0.03	410
$\mathbf{7}^-$	336 ± 100	0.65 ± 0.09	512
$\mathbf{8}^-$	35.4 ± 3.4	0.56 ± 0.07	63
$\mathbf{9}^-$	31.2 ± 4.3	0.74 ± 0.08	43

[a]Selectivity index is the ratio between K_i (CAII) and K_i (CAIX).

All compounds demonstrated inhibitory activity against CAIX, with corresponding inhibition constants (K_i values) in the low nanomolar to subnanomolar range, as well as selectivity toward CAIX over CAII. Compounds $\mathbf{1}^-$ and $\mathbf{2}^-$, with six-atom linkers between the cobaltacarborane cluster and the sulfamide group, exhibited nanomolar potency toward CAIX. The lower potency of $\mathbf{1}^-$ compared to $\mathbf{2}^-$ could be attributed to the known tendency of a diethylene glycol spacer connected to borate anions to form a rigid, crown ether-like arrangement upon complexation with alkali metal cations.[45−47] This effect decreases the solubility of the compounds and increases their tendency to aggregate[46,48−50] and thus might limit interactions with the enzyme active site. The relatively low inhibitory activity of $\mathbf{3}^-$ toward CAIX could be explained by the combined effect of suboptimal linker length with possible unfavorable interactions of the methoxy substituent present at the B(8′) atom of the cluster.

Elongation of the pendant arm through the incorporation of an aminoethyl unit in **4** led to an almost 3-fold increased affinity for CAIX. Binding the methylene sulfamide functional group to C(1) atom in $\mathbf{5}^-$ resulted in an approximately 60-fold decrease in K_i. Inhibitory potency increased further when the linking group was elongated by one additional methylene unit in $\mathbf{6}^-$ (K_i = 63 pM). An ethylene linker between the metallacarborane cage and sulfamide group seemed optimal for high affinity toward the CAIX isoform. Further elongation to a propylene chain, as in $\mathbf{7}^-$, resulted in a 1-order-of-magnitude higher K_i. The presence of a second polar alkylsulfamide group on the cage also reduced potency. We observed a slight difference in K_i values between $\mathbf{8}^-$ and $\mathbf{9}^-$; however, these compounds represent different diastereoisomers. Overall, the compounds were selective for CAIX over CAII, with selectivity indices ranging from 42 to 518. The cobaltacarborane compounds displayed roughly 6-order-of-magnitude lower K_i values and an almost 28-fold increase in selectivity for CAIX compared to the previously explored series of single-cage carborane inhibitors.[22]

Crystal Structures and Insight into Inhibitor Interactions in the CAIX Active Site. Three compounds with highest inhibitory potency and selectivity toward CAIX were subjected to X-ray diffraction studies to explore their interactions with the CAIX active site. Compounds $\mathbf{5}^-$, $\mathbf{6}^-$, and $\mathbf{7}^-$ were cocrystallized with a CAIX mimic-CAII

DOI: 10.1021/acs.jmedchem.9b00945
J. Med. Chem. 2019, 62, 9560−9575

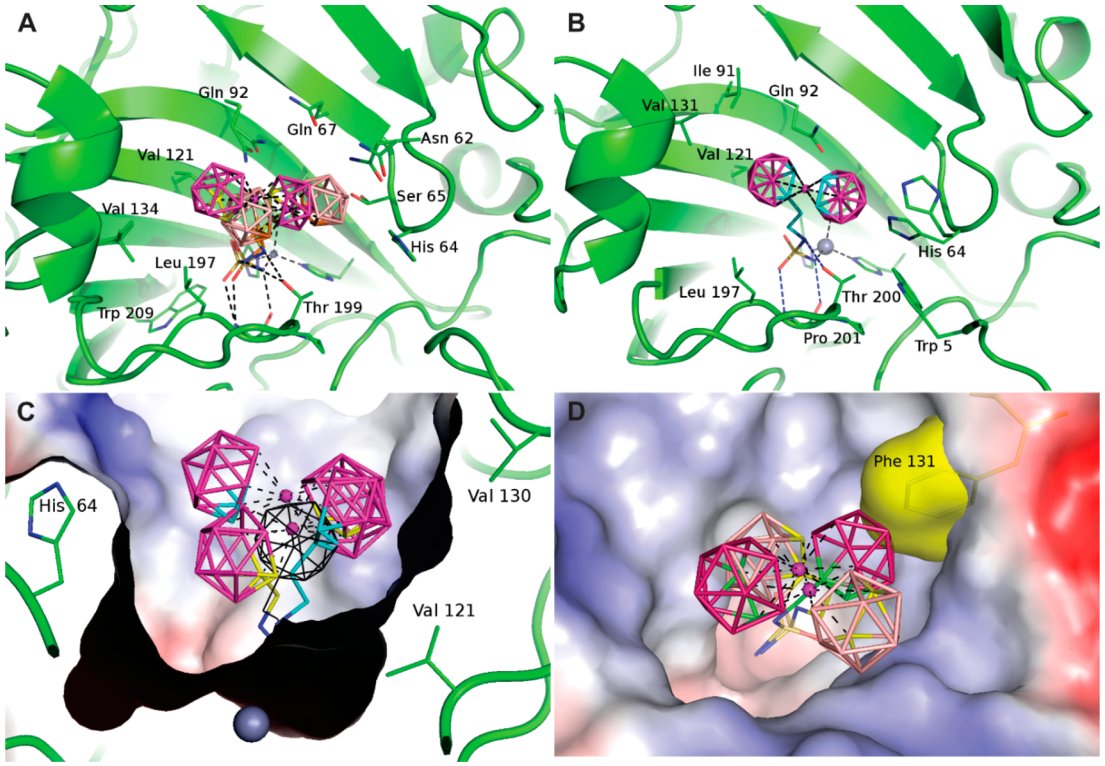

Figure 1. Structures of 5^- (A) and 6^- (B) bound to the CAIX active site. Compounds are depicted in stick representation with the cobalt atom shown as a maroon sphere. The protein is shown in green cartoon representation with residues interacting with 5^- and 6^-, respectively, highlighted as sticks and labeled. Coordination bonds with the cobalt atom are shown as black dashed lines. (C) Side view of the CAIX active site, which is represented by its solvent accessible surface colored by electrostatic potential (red for negative, blue for positive), and superposition of 5^- (carbon atoms in yellow; only the dominant alternative conformation is shown for clarity), 6^- (carbon atoms in turquois). (D) Top view into the CAIX active site, which is represented by its solvent accessible surface. Pose of 6^- in CAIX (carbon atoms in turquois) is superposed with pose of 6^- docked into the CAII (carbon atoms in yellow). Phe131 in CAII is represented by yellow sticks and surface.

containing the following seven amino acid substitutions: A65S, N67Q, E69T, I91L, F130V, K169A, and L203A. This variant is often used in structural studies, as it retains the good crystallization properties of CAII, while the active site resembles that of CAIX.[51,52] Two crystal structures determined at an atomic resolution of 1.1 Å confirmed the specific binding of 5^- and 6^- in the active site of CAIX and compounds could be unambiguously modeled into well-defined electron density maps (Supporting Information Figure S1). Crystal structure of CAIX mimic in complex with 7^- determined at resolution 1.74 Å revealed that the electron density map for distal part of the compound is missing and that the position of the cage cannot be modeled due to dynamic or static disorder (Supporting Information Figure S1). The structure thus was not refined.

The electron density map indicated that compound 5^- assumes two alternative conformations, while derivative 6^- is bound in a single mode (Figure 1A). The sulfamide moiety is deeply buried in the active site, where it makes polar interactions with the zinc ion and residues His94, His96, and His119 located at the bottom of the active site cavity. These binding interactions are similar to those reported for organic sulfamide-containing inhibitors.[53−55] The cobaltacarborane cluster of 5^- occupies two alternative binding sites. In the preferred conformation 1, it makes 84 interatomic contacts with Asn62, Ser65, Gln67, Leu91, Gln92, His94, Val130, Val134, Leu197, and Thr198−199. In conformation 2, it makes 147 interactions with Trp5, Asn62, His64, Ser65, Gln67, Gln92, His94, Leu197, Thr198−199, and Pro200. The cobaltacarborane cluster of 6^- makes 89 interatomic contacts with His3, Trp5, Asn62, His64, Leu91, Gln92, Val121, Val130, Leu197, Thr198−199, and Pro200. The efficient interaction of the bulky cobaltacarborane cage with the enzyme active site observed in the crystal structures helps explain the high inhibitory affinity of 5^- and 6^-.

One dicarbollide ligand from the cobalt bis(dicarbollide) sandwich of both 5^- and 6^- interacts with a hydrophobic pocket formed by Leu91, Val130, and Val134. The second dicarbollide of 5^- is buried within a hydrophilic pocket loop located deeper in the enzyme cavity formed by Asn62-Ser65. Due to the longer linker in 6^-, the second dicarbollide ligand interacts with a hydrophilic patch formed by the N-terminal part of the protein. Extensive interaction of the cage of 6^- with a hydrophobic pocket formed by Leu91, Val130, and Leu140 explains its subnanomolar affinity toward CAIX. The linker between sulfamide group and carboranes cage in 6^- seems to be of optimal length for proper positioning of the cage into this hydrophobic pocket. Further extension of linker in 7^- leads to a decrease in K_i value by 1 order of magnitude (Table 1). The fact that position of cage could not be modeled in the crystal structure of 7^- complex indicates that linker elongated by one group extends the cage toward the opening of the active site, where it forms unspecific interaction with surface or is completely disordered.

Interaction of cage of 6^- with a hydrophobic pocket containing Val130 residue also provides structural explanation for high selectivity of this compound toward CAIX. This hydrophobic pocket is not present in CAII. CAII has a phenylalanine residue (Phe131) at the position corresponding

DOI: 10.1021/acs.jmedchem.9b00945
J. Med. Chem. 2019, 62, 9560−9575

to Val130, and its bulky side chain changes the shape of the active site. Docking studies of 6^- into CAII revealed less favorable binding mode of the cage of 6^- in CAII active site (Figure 1D).

Preferential Reduction of Malignant Cells Survival in Vitro. We tested the toxicity of compounds 1^- to 9^- in the form of Na^+ salts (with exception of zwitterionic compound **4**) under normoxic conditions on a panel of 11 cell lines derived from malignant tissues and two prototypes of nonmalignant fibroblast cell lines using a standard MTT assay (Table 2). Additionally, we also included U-104, a positive CAIX inhibitor currently in clinical trials,[56] and GB-18, the sodium salt of parent cobalt bis(dicarbollide) ion, as positive and negative controls, respectively. Of all the cobaltacarboranes, **4** showed the highest in vitro cytotoxicity across the cell line panel with no selectivity for malignant over nonmalignant cells, possibly due to off-target effects (Table S3). The IC_{50} values of most of the compounds varied among the cell lines. Compounds such as 3^-, 5^-, 6^-, 7^-, 8^-, and 9^- showed moderate cytotoxicity in one or more tumor cell lines regardless of histogenetic origin and drug resistance characteristics in comparison to either MRC-5 or BJ fibroblasts (Table S3). Interestingly, MDCK cells regardless of CAIX expression were not sensitive to cobaltacarborane cytotoxicity (except **4**), most likely reflecting their nonmalignant and/or non-human origin. U-104 and GB-18 did not show any cytotoxicity across the cell line panel. The lack of cytotoxic effect of U-104 in 2D tumor cell cultures presumably resulted because of the absence of CAIX expression under normoxia (Figure S2).

To evaluate the growth inhibitory activity in pathophysiologically relevant in vitro tumor models, we measured the time-dependent effect of compounds on MCSs of HT-29 and HCT116 cells that show high and low levels,[56] respectively, of hypoxia-induced CAIX (Figure S2A). Compound 6^- with highest inhibitory potency toward CAIX and its closest analog 8^- containing an additional sulfonamide group were selected for MCS and subsequent biological studies. In parallel, we also determined the effect of U-104 on MCSs and the cytotoxicity of 6^- and 8^- in 2D cultures of both the cell types after 3−7 days of treatment in normoxia. First, there was no significant change in the cytotoxicity of 6^- after 7 days of treatment in 2D cultures of both cell types; however, a longer treatment time increased 8^- cytotoxicity in HCT116 only (Figure S2B). Next, treatment with both compounds resulted in a time-dependent decrease in the size of MCSs of both the cell lines; however, the fold change in IC_{50} values of 6^- and 8^- was more pronounced in MCSs of HT-29 cells (Figure S2B). U-104 showed a similar time-dependent effect on MCS growth (Figure S2C). The time-dependent effect of 6^- and 8^- on MCS size was proportional to a time-dependent increase in CAIX expression in MCSs in the absence of inhibitors, particularly in HT-29 cell MCSs (Figure S2D,E). Overall, these data suggest that both 6^- and 8^- specifically target CAIX-expressing MCSs and that MCSs are a more reliable model to study cellular effects of CAIX inhibition.

Effect of Cobaltacarborane Inhibitors on the Intracellular Distribution of CAIX. To determine the interaction of 6^- and 8^- with CAIX in HT-29 cells, the cellular distribution of the compounds was determined by Raman spectroscopy followed by immunofluorescence to measure CAIX expression (Figure 2). The presence of 6^- and 8^- was detected at saturating concentrations in order to increase detection limit of compounds using specific marker bands at

Table 2. Cytotoxicity of Compounds against a Panel of Cell Lines in 3-Day MTT Assay[a]

	cell											
line	MRC-5	BJ	CCRF-CEM	CEM-DNR	K652	K562-TAX	A549	HCT116	HT-29	HeLa	4T1-luc	MDCK-CAIX	MDCK-NEO
1-	>100	>100	95 ± 5	>100	>100	>100	>100	>100	>100	>100	>100	>100	>100
2-	>100	>100	90 ± 6	95 ± 8	99 ± 2	96 ± 4	>100	85 ± 3	>100	>100	70 ± 6	94 ± 11	88 ± 18
3-	78 ± 1	76 ± 3	62 ± 18	75 ± 8	74 ± 4	55 ± 5	95 ± 4	69 ± 3	>100	89 ± 17	99 ± 4	>100	>100
4-	27 ± 5	65 ± 4	17 ± 1	48 ± 8	18 ± 1	17 ± 1	34 ± 8	17 ± 0	12 ± 1	12 ± 1	13 ± 1	13 ± 0	13 ± 0
5-	93 ± 7	>100	85 ± 23	100 ± 0	99 ± 2	66 ± 8	>100	75 ± 4	>100	90 ± 15	>100	>100	>100
6-	98 ± 4	>100	67 ± 3	86 ± 4	>100	74 ± 2	85 ± 3	50 ± 1	78 ± 9	99 ± 3	>100	>100	>100
7-	>100	>100	71 ± 6	44 ± 7	98 ± 2	67 ± 3	>100	52 ± 3	>100	>100	>100	>100	>100
8-	96 ± 7	>100	69 ± 7	69 ± 7	80 ± 10	100 ± 1	>100	79 ± 1	>100	>100	>100	>100	>100
9-	>100	>100	69 ± 10	76 ± 5	75 ± 4	99 ± 3	>100	88 ± 14	>100	>100	>100	>100	>100
U-104	>100	>100	>100	>100	>100	>100	>100	>100	>100	>100	>100	>100	>100
GB-18	>100	>100	33 ± 3	>100	>100	>100	>100	>100	>100	>100	-	>100	>100

[a] IC_{50} (μM) values of compounds 1^-−9^- are presented as the mean ± SD of four independent experiments. The IC_{50} values of U-104[56] and GB-18 are the mean ± SD of four values from one independent experiment.

DOI: 10.1021/acs.jmedchem.9b00945
J. Med. Chem. 2019, 62, 9560−9575

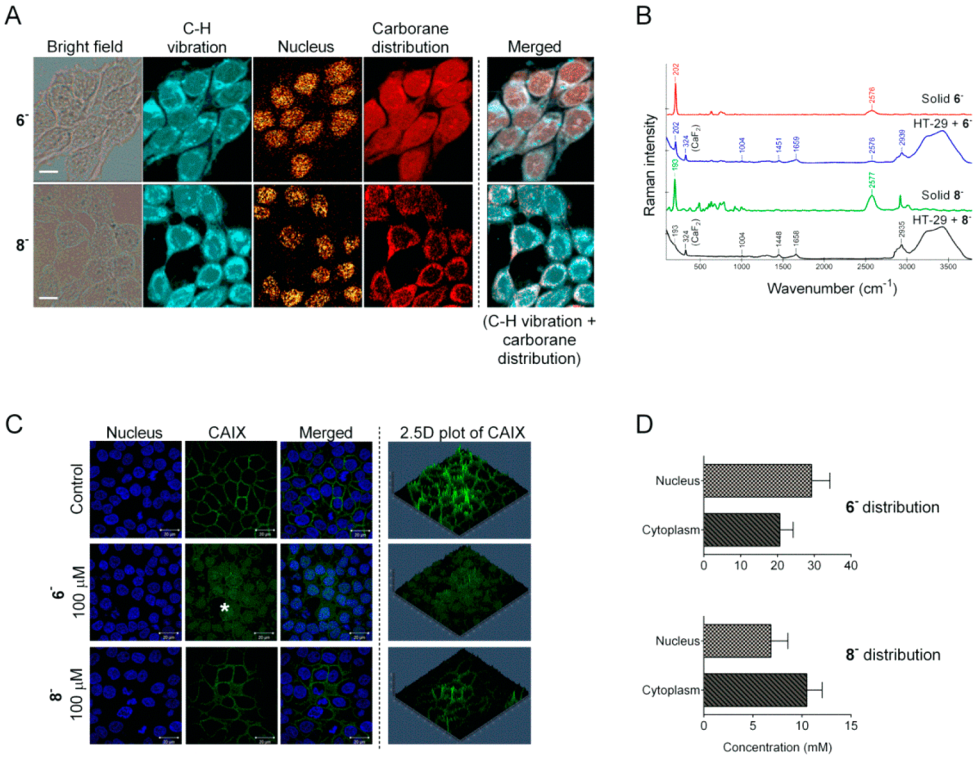

Figure 2. Raman spectra showing the distribution of 6^- and 8^- in HT-29 cells. (A) HT-29 cells treated with 100 μM sodium salts of 6^- and 8^- for 12 h. From left to right: microscopic bright-field image (scale bar 10 μm); distribution of C−H stretching vibrations at 2800−2950 cm^{-1}; distribution of nucleic acid marker at 790 cm^{-1}; distribution of 6^- and 8^- according to Raman marker bands at 202 and 193 cm^{-1}, respectively; merged image of C−H vibrations and carborane distribution. (B) Raman spectra of 6^- and 8^- in solid form are shown in red and green, respectively. The typical appearance of 6^- and 8^- Raman marker bands on the background of the HT-29 cell fingerprint is in blue and black, respectively. The band at 324 cm^{-1} corresponds to CaF_2 substrate. (C) Images showing the changes in expression of CAIX in HT-29 cells treated with 100 μM 6^- and 8^- for 12 h. Objective: 100×. (D) Average concentration (mM) of 6^- and 8^- in the nucleus and cytoplasm of HT-29 cells based on Raman measurements.

202 and 193 cm^{-1}, respectively, in Raman maps of treated cells (Figure 2A,B). This marker corresponds to the characteristic vibration between a cobalt atom and dicarbollide ligands. Immunostaining of HT-29 grown under hypoxic conditions showed that 6^- has a greater effect on CAIX localization compared to cells treated with 8^- and untreated cells (Figure 2C). CAIX was redistributed from the cell surface to the cytoplasm and nucleus of inhibitor-treated cells. Raman spectroscopy corroborated these results, indicating the presence of more 6^- in the nucleus than cytoplasm of treated cells (Figure 2A,B). On the other hand, 8^- was preferentially present in the cytoplasm, in agreement with the cytoplasmic membrane localization of CAIX upon treatment with 8^- (Figure 2A,B). Quantitative comparisons of Raman intensity showed that the signal intensity for 6^- corresponds to a nearly 29.3 ± 5.0 mM concentration in the nucleus and 20.7 ± 3.6 mM in the cytoplasm (Figure 2D). The signal for 8^- corresponds roughly to 6.8 ± 1.7 mM in nuclei and 10.5 ± 1.6 mM in the cytoplasm (Figure 2D), indicating that approximately 5-fold more 6^- than 8^- is localized in nuclei and only 2-fold more in the cytoplasm.

Facilitated Doxorubicin (DOX) Penetration into MCSs observed in the Presence of CAIX Inhibitors 6^- and 8^-. As treatment with 6^- affected CAIX distribution in 2D cultures (Figure 2C), we next followed CAIX expression and distribution in MCSs of HT-29 cells treated with 6^- and 8^- in the form of Na^+ salts and determined whether CAIX inhibition facilitates the penetration of DOX, a prototypal anticancer molecule with fluorescent properties. To analyze the changes in CAIX expression, MCSs were treated for 3 days with 0.5× and 1× IC_{50} concentrations (Figure S2). Western blot analysis of MCS lysates indicated that both 6^- and 8^- (at 60 μM concentration) significantly downregulated the expression of CAIX in MCSs (Figure 3A). Immunostaining of MCSs showed that 6^- changed the distribution of CAIX in cells (Figure 3B), similar to what we observed in 2D cultures (Figure 2C).

Redistribution of CAIX may affect the composition of the extracellular matrix via modulation of matrix metalloproteinases activities,[57] resulting in aberrant penetration of cytotoxic drugs into tissues.[58,59] To test the hypothesis that 6^- and 8^- affect penetration and/or accumulation of cytotoxic drugs, MCSs were treated with the fluorescent anticancer compound, DOX, in combination with either 6^- or 8^- and imaged every 10 min for 120 min by light-sheet fluorescence microscopy. Treatment with 6^- and 8^- greatly facilitated the accumulation of DOX (Figure 3C,D). As the increased anti-CAIX activity of 6^- is associated with the presence of an ethylene sulfamide functional group, we next treated the MCSs with DOX in the presence of cobalt bis(dicarbollide) ion (GB-18), a compound lacking the alkyl sulfamide functional group. This ion did not have a major effect on DOX penetration (Figure 3D). In addition to increasing DOX penetration over time, 6^- affected MCS integrity (Figure 3D). A line plot across the MCS surface at 50 μm depth indicates an increased accumulation of DOX in MCSs treated with 6^- (Figure 3E). Altogether, our data reveal

DOI: 10.1021/acs.jmedchem.9b00945
J. Med. Chem. 2019, 62, 9560−9575

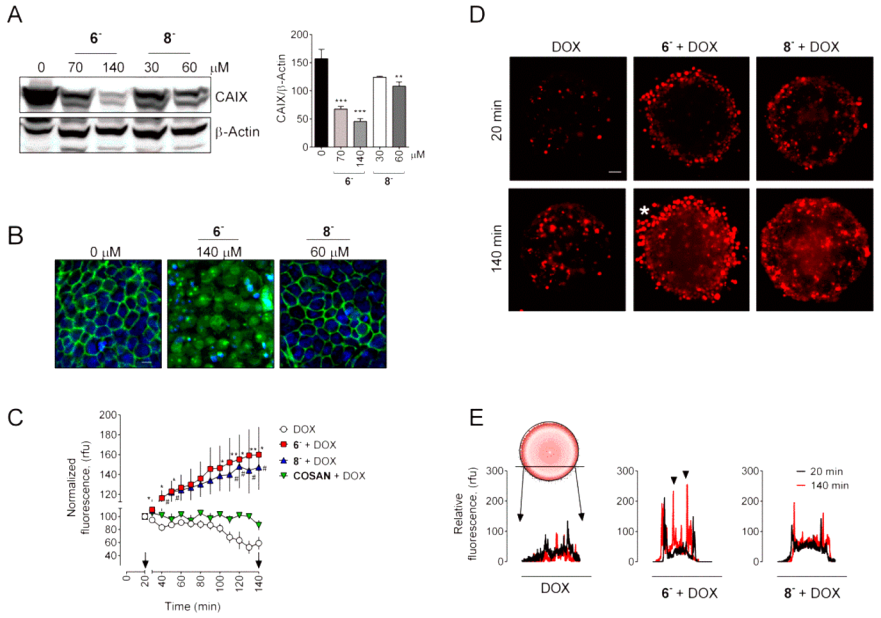

Figure 3. Effect of 6^- and 8^- on CAIX expression and DOX accumulation in MCSs of HT-29 cells. (A) CAIX expression in MCSs treated with 6^- or 8^- at 0.5× and 1× IC_{50} concentrations (Figure S2) for 3 days with the indicated concentrations. Data are the mean ± SEM from three to five independent experiments: ***$p < 0.001$, **$p < 0.01$ comparing treated to untreated controls (0 μM). (B) Immunostaining of drug-treated MCSs shows the downregulation of CAIX by 6^-. Images are enlarged sections of the MCS surface. Nuclei are stained blue with Hoechst 33342; 5× objective, scale bar 50 μm. (C) Graph showing the rate of DOX accumulation in MCSs treated with DOX only, 430 μM 6^- in combination with DOX (6^- + DOX), 180 μM 8^- in combination with DOX (8^- + DOX), and 430 μM cobalt bis(dicarbollide) ion in combination with DOX [cobalt bis(dicarbollide) ion + DOX] 140 min after the beginning of the experiment (120 min of treatment; the treatment period is indicated by arrows). Data are the mean ± SEM of at least two MCSs per treatment type from three independent experiments: **$p < 0.01$, *$p < 0.05$ comparing 6^- + DOX to DOX only and **$p < 0.01$, *$p < 0.05$ comparing 8^- + DOX to DOX only, with one-way ANOVA with Tukey's multiple comparison test. The DMSO concentration in treated samples in (A)−(C) was always below 0.5%. (D) Representative images of DOX accumulation at 50 μm z-plane height in MCSs treated with DOX alone or in combination with 6^- or 8^- at the indicated time points. Note the effect of 6^- on MCS integrity (indicated by an asterisk); 5× objective, scale bar 20 μm. (E) A plot of DOX intensity along the line profile in images from (D) shows increased accumulation of DOX in the interior of MCSs treated with 6^- (indicated by arrowheads).

Table 3. Pharmacological Properties of 6^- and 8^- Determined by in Vitro and in Vivo ADME Assays

	metabolism			permeability			
	in vitro			in vitro		in vivo	
	in vitro			PAMPA		MDR1-MDCK	Caco-2
compd	plasma stability (category)	plasma protein binding (% bound)	microsomal stability (clearance)	category	% recovery	CNS (−ive/+ive)	category
6^-	stable	99.8	low	medium	86.4	CNS: −ive efflux ratio: 1.7 active efflux: no % recovery: 38.1	low efflux ratio: 0.8 active efflux: no % recovery: 20.0
8^-	stable	99.3	low	medium	72.7	CNS: −ive efflux ratio: 14.1 active efflux: yes % recovery: 87.3	low efflux ratio: 42.0 active efflux: yes active efflux: yes

better penetration of DOX in MCSs co-treated with cobaltacarborane CAIX inhibitors and suggest the potential for future synergistic combinations to combat human cancers.

In Vitro Pharmacological Properties of 6^- and 8^-. Results from ADME assays revealed that sodium salts of compounds 6^- and 8^- are stable in the presence of plasma proteins and are very slowly metabolized by microsomes (Table 3). This is evident from the low value of intrinsic clearance, which indicates that there is a high probability that the compounds will not be primarily metabolized in the liver. Both 6^- and 8^- bound to plasma proteins with more than 99% affinity. The passive diffusion mechanism for both compounds through the PAMPA membrane was classified as medium compared with other commonly used drugs. The limited intercellular diffusion of 6^- and 8^- may further increase the CAIX/CAII specificity index because intracytoplasmic CAII protein will be less available for the cobaltacarborane inhibitor. The compounds showed poor permeability in MDCK-MDR1 cells, indicating a low potential for penetration through the blood−brain barrier. Furthermore, the low permeability of 6^- and 8^- in Caco-2 cells suggests that the compounds are likely not suitable for oral administration due to their poor absorption through the intestine.

DOI: 10.1021/acs.jmedchem.9b00945
J. Med. Chem. 2019, 62, 9560−9575

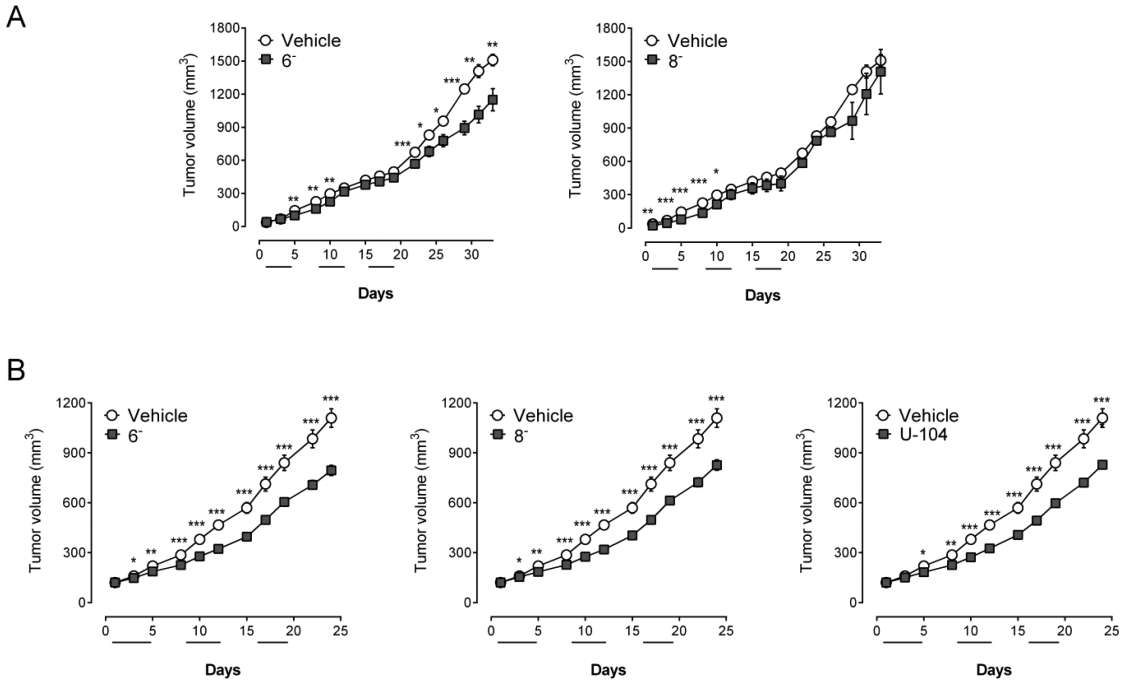

Figure 4. In vivo antitumor activity of **6**$^-$ and **8**$^-$. (A) Graphs showing the effect of **6**$^-$ and **8**$^-$ salt on tumor size in female BALB/c mice orthotopically transplanted with 4T1-12B cells over a period of 33 days. (B) Graphs showing the effect of **6**$^-$, **8**$^-$, and U-104[56] over a period of 24 days in female SCID mice bearing subcutaneously transplanted HT-29 cell tumors. Mice were administered **6**$^-$ and **8**$^-$ twice and once per day, respectively, at a dose of 62.5 mg/kg. U-104 was administered once per day at a dose of 38 mg/kg for 3 weeks. Dosing schedules are shown by the black solid lines in the *x*-axes. The doses of **6**$^-$ and **8**$^-$ were chosen based on their pharmacological properties, whereas U-104 dose was selected based on the published report.[56] Data in (A) and (B) are the mean ± SEM of typically 20 tumors transplanted to 10 animals per group: ***$p < 0.001$, **$p < 0.01$, *$p < 0.05$ comparing vehicle-treated to drug-treated tumors, Student's *t*-test, paired.

The plasma concentration−time profiles of **6**$^-$ and **8**$^-$, following ip administration to NMRI mice at a maximum tolerated dose (MTD) of 125 mg/kg were determined over 36 h. The compounds were administered as sodium salts in a vehicle comprising 10% DMSO. Apart from initial symptoms of somnolence following **6**$^-$ and piloerection following **6**$^-$ and **8**$^-$, there were no visible signs of major toxicity on animal behavior, appearance, or body weight. The maximum concentrations (C_{max}) of boron and cobalt in serum at the MTD were 661 μM for **6**$^-$ at 3 h and 404 μM for **8**$^-$ at 6 h. The serum half-life ($t_{1/2}$) of **6**$^-$ was 4.8 h, and it was 15.6 h for **8**$^-$. The MTD for repeated dose toxicity delivered once (**8**$^-$) or twice (**6**$^-$) daily for 5 days in two cycles with 2 days in between cycles was 62.5 mg/kg for both compounds.

Antitumor Activity of Compounds 6$^-$ and 8$^-$ in Mouse Models of Mammary and Colorectal Tumors. Next, the in vivo antitumor activity of Na.**6** and Na.**8** in two mouse models was explored: (1) syngenic mouse mammary tumors of 4T1-12B cells orthotopically transplanted into the mammary glands of Balb/c mice and (2) human colorectal cancer HT-29 cells xenotransplanted into SCID mice. Treatment with **6**$^-$ and **8**$^-$ significantly decreased the 4T1-12B tumor size over the first 10 days. A significant effect on tumor size was also observed after 22−32 days of treatment with **6**$^-$ compared to vehicle-treated animals (Figure 4A).

Both **6**$^-$ and **8**$^-$ significantly reduced the tumor size compared to vehicle-treated controls in SCID mice xenotransplanted with HT-29 over the entire period of the experiment (Figure 4B). To better compare these effects, we included U-104 that was reported to significantly reduce tumor growth in NOD/SCID mice orthotopically implanted with breast MDA-MB-231 cancer cells.[56] Both **6**$^-$ and **8**$^-$ displayed a similar antitumor activity as U-104, and tumor sizes after 24 days in mice treated with **6**$^-$, **8**$^-$, and U-104 were 68%, 75%, and 87% in comparison to vehicle-treated tumors, respectively.

CONCLUSION

The cobalt bis(dicarbollide) cluster ion serves as a convenient hydrophobic inorganic building block for the construction of CAIX inhibitors due to the possibility of peripheral substitution with sulfamide groups. Compared to smaller carborane frameworks, the cobalt bis(dicarbollide) ion provides the desired space-filling properties and introduces additional interactions with the enzyme active site, leading to a dramatic improvement in inhibition efficacy and selectivity for CAIX. The observed K_i values ranged from nanomolar to subnanomolar and are several orders of magnitude lower than those for corresponding alkylsulfamidodicarbaboranes.[22] The cobalt bis(dicarbollide) compounds also have 2−3 order-of-magnitude higher inhibition potency than recently reported metallocene-sulfonamides.[60] Furthermore, the CAIX/CAII selectivity index reached a value of approximately 500 for the best inhibitor of the series, indicating specific inhibition of CAIX. X-ray structural analyses of the cobaltaborane-CAIX mimic complexes revealed that the length of the linker between the sulfonamide anchor and the cluster is important for orienting the ionic cluster for optimal interaction with hydrophobic and hydrophilic pockets in its proximity.

Two compounds, **6**$^-$ and **8**$^-$, were selected for further studies including ADME analysis, pharmacokinetics, and antitumor activity experiments. Compound **6**$^-$ had an extremely high affinity toward CAIX (K_i = 63 pM) and high selectivity for CAIX over CAII (selectivity index of 410).

DOI: 10.1021/acs.jmedchem.9b00945
J. Med. Chem. 2019, 62, 9560−9575

Binding of 6^- and 8^- to CAIX in cell cultures was confirmed by a combination of immunostaining and Raman spectroscopy-based methods. Interestingly, 6^- affected CAIX localization within the cell and the amount of CAIX present in the cell. CAIX was detected in high amounts in the cytoplasm and nuclei of 6^--treated HT-29 cells. We presume that 6^- affects proteins involved in an excretory mechanism that results in the active transport or passive diffusion of 6^- CAIX complex (55 kDa) via the nuclear pore into the nucleus, where it is detected by the anti-CAIX antibody and Raman spectrometry.

Interestingly, both 6^- and 8^- facilitated the accumulation of DOX in MCSs. Moreover, 6^- also affected MCS integrity. This suggests that inhibition of CAIX expression, activity, or distribution by metallacarboranes may facilitate the penetration of other anticancer drugs that are affected partially by tumor pH and/or composition of the extracellular matrix. ADME analysis revealed that 6^- and 8^- are stable in plasma and bind to plasma proteins with more than 99% affinity. These compounds penetrate cells by passive diffusion and have low predicted absorptivity by the gastrointestinal tract and low BBB penetration potential, as indicated by cell permeability assays using MDCK-MDR1 and Caco-2 cells. Compounds 6^- and 8^- displayed low in vitro and in vivo toxicity to normal tissues and a sufficiently high concentration in serum after administration. The repeated dose of 6^- greatly reduces the tumor size in mice transplanted with 4T1-12B breast cancer cells. Moreover, 6^- and 8^- also reduced tumor size in SCID mice xenotransplanted with HT-29 cells, similar to the reference CAIX inhibitor U-104 currently under clinical trials.[56] In conclusion, cobaltacarborane CAIX inhibitors have the potential for further development as antitumor agents. More generally, due to favorable pharmacological properties, carboranes should be considered for further research and development as drug-like chemical structures.

EXPERIMENTAL SECTION

Synthesis: General. The starting cesium salt of cobalt bis(dicarbollide) was purchased from Katchem Ltd., Czech Republic. Tetrahydrofuran (THF) and 1,4-dioxane were dried with sodium diphenyl ketyl and distilled prior to use. Acetonitrile was dried over molecular sieves 4 Å (Fluka). Sulfamide (97%) was purchased from Maybridge-Thermo Fisher Scientific and dried in a vacuum. Butyllithium in hexane and ethylene diamine were purchased from Aldrich. Other chemicals and solvents were obtained from Aldrich, Merck Lachema a.s. and Penta Ltd., Czech Republic, and used without purification. Analytical TLC was carried out on Merck RP-18 F_{254} TLC plates in 50% aqueous MeOH. Unless otherwise specified, column chromatography was performed on high purity silica gel (Merck grade, type 7754, 70−230 mesh, 60 Å). All reactions were performed using standard Schlenk type vacuum or inert-atmosphere techniques. Some operations, such as column chromatography and crystallization, were carried out in the air.

The identities of all the reported compounds were unambiguously verified by a combination of ^{11}B, ^1H, and ^{13}C NMR spectral data (complete assignment of the resonances), mass spectrometry (two decimal place resolution or HRMS), elemental analysis, TLC, and other methods. The purity was also assayed by a previously developed analytical HPLC method with DAD detection,[61] under chromatographic conditions specified in the paragraph below and was ≥95% for all compounds. Unless otherwise specified, the NMR and MS data are given for the sodium salts, which were used as end products for cell assays or in vivo experiments. For chemical analyses and melting points, the Me_4N^+ salts were used.

Melting points were determined in sealed capillaries on a BŰCHI Melting Point B-545 apparatus and are uncorrected.

Instrumental Techniques. ^1H, ^1H,[62] $^1H\{^{11}B_{selective}\}$, ^{13}C, and ^{11}B NMR spectra were measured on a Varian Mercury 400^{Plus} instrument. The spectra of all compounds were measured immediately after dissolution in deuterated solvent, usually acetonitrile-d_3 or acetone-d_6. ^{11}B NMR (128 MHz) chemical shifts are given in ppm to high-frequency (low field) to $F_3B{\cdot}OEt_2$ as the external reference. Residual solvent ^1H resonances were used as internal secondary standards. Coupling constants $^1J(^{11}B-^1H)$ were taken from resolution-enhanced ^{11}B spectra with a digital resolution of 2 Hz. The NMR data are presented in the text as follows: ^{11}B NMR, ^{11}B chemical shifts δ in ppm, multiplicity, coupling $J(^{11}B-^1H)$ constants in Hz. Signal assignments are based on $[^{11}B-^{11}B]$ COSY NMR spectroscopy. ^1H NMR (400 MHz) and ^{13}C NMR (100 MHz): chemical shifts δ in ppm relative to Me_4Si (0 ppm) as the external standard, coupling constants J(H, H) in Hz. The chemical shifts corresponding to B−H resonances were obtained from $^1H\{^{11}B_{selective}\}$ NMR spectra. In $^1H\{^{11}B\}$ spectra the δ_{B-H} values and peak assignments were analyzed from $^1H\{^{11}B_{selective}\}$ experiments.

Mass spectrometry measurements were performed on Thermo Fisher Scientific LTQ Orbitrap XL (HRMS) and Thermo-Finnigan LCQ-Fleet ion trap instruments using electrospray ionization (ESI) for ionic species with detection of negative or positive ions. For ESI, samples dissolved in acetonitrile (concentrations approximately 100 $ng{\cdot}mL^{-1}$) were introduced to the ion source by infusion. Molecular ions $[M]^-$ were detected for all univalent anions as base peaks in the spectra. Full agreement between the experimental and calculated isotopic distribution pattern was observed for all isolated compounds. The isotopic distribution in the boron plot of all peaks was in complete agreement with the calculated spectral pattern. The data are presented for the most abundant mass in the boron distribution plot (100%) and for the peak on the right side of the boron plot corresponding to the m/z value.

For HPLC, a Merck-Hitachi LaChrom series 7000 HPLC system equipped with a DAD 7450 detector and a L7250 programmable autosampler was used. Anion separation was carried out according to a previously reported ion-pair RP method for separation of hydrophobic borate anions[61] on a RP Separon SGX C8 column, 7 μm (250 mm × 4 mm i.d.), Tessek Prague. The mobile phase was 4.5 mmol of hexylamine acetate in 58% aqueous CH_3CN (pH 6.0) (sulfamides and amines) and 49% aqueous CH_3CN (hydroxy derivatives) (pH 6.0) at a flow rate of 1 mL. Samples with concentration of approximately 1 $mg{\cdot}mL^{-1}$ in the mobile phase were injected. DAD detection was carried out at fixed wavelengths 235, 260, 285, and 312 nm; samples of concentration of approximately 1 $mg{\cdot}mL^{-1}$ in the mobile phase were injected. For metallacarborane amines and overall purity assays of sulfamides, a mobile phase containing 58% aqueous CH_3CN was used. Purity of all compounds that was determined by HPLC was better than 95%. For HPLC traces of products 1^- to 9^-, see Supporting Information.

Elemental analyses were performed on a Thermo Scientific FlashSmart organic elemental analyzer using a V_2O_5 catalyst weighted with the sample for combustion of the samples in oxygen. All compounds for EA were converted to respective Me_4N^+ salts and were dried for 12 h in vacuum at 80 °C before analyses.

Synthetic Procedures. The compounds (compounds 1^- to 9^- in Scheme 1) were prepared from their respective amine or ammonium derivatives. For more information about the overall reaction pathways including the ways to the corresponding amines, see Schemes S1−S5 in Supporting Information. The transamination reactions of terminal amino groups (with the exception of 3^- obtained by direct reaction) leading to sulfamide substitution were carried out in refluxing dioxane in the presence of K_2CO_3 or Na_2CO_3. Product isolation was typically achieved by precipitation with an excess of aqueous NMe_4Cl, liquid chromatography, and/or crystallization of crude products from CH_2Cl_2−hexane. For in vivo experiments, the NMe_4^+ salts of the new compounds were converted to Na^+ salts by metathesis (see Supporting Information).

8-Sulfamido-1,4-diethyleglycolyl-3,3′-*commo*-bis(decahydro-1,2-dicarba-3-cobalta(III)-*closo*-dodecabor)ate (1-), (Na1). The known[63] zwitterionic compound $[8\text{-}H_3N\text{-}(C_2H_4O)_2\text{-}$

DOI: 10.1021/acs.jmedchem.9b00945
J. Med. Chem. 2019, 62, 9560−9575

$(1,2\text{-}C_2B_9H_{10})_2$-3,3′-Co(III)] was prepared by recently updated procedure in which the dioxane derivative[38] was treated with ammonia in THF.[36] This compound (101 mg, 0.23 mmol) was dissolved in 1,4-dioxane (5 mL) under nitrogen. Solid sulfamide ($H_2NSO_2NH_2$, 224 mg, 2.33 mmol) followed by anhydrous Na_2CO_3 (246 mg, 2.32 mmol) was added, and the slurry was then vigorously stirred and refluxed for 2 h. The reaction was periodically monitored by TLC (CH_3CN−CH_2Cl_2, 1:3) and by MS ESI, and solvents were evaporated under reduced pressure when the starting derivative disappeared. The solids were treated with acetonitrile (5 mL), the resulting slurry was filtered, and the filtrate was evaporated under reduced pressure. The orange solid was dissolved in diethyl ether (10 mL) and treated in an extraction funnel with diluted HCl (3 M, 3 × 10 mL) and then by water (2 × 10 mL). The organic layer was separated, and the crude product was dissolved in a mixture of CH_2Cl_2 and CH_3OH (10:1 bv, 22 mL). The resulting solution was layered with hexanes and left to crystallize overnight. The semisolid product was decanted and dried in a vacuum at 50 °C. It solidified as an orange foamy solid. The mother liquors were partially evaporated and decanted, and the resulting solid was combined with the first crystallization crop. Overall yield Na**1**·H_2O: 110 mg (91%). ^{1}H NMR (400 MHz; CD_3CN, Me_4Si) δ_H/ppm: 4.15 (2 H, s, C$H_{carborane}$), 4.06 (2 H, s, C$H_{carborane}$), 3.60 (2H, t, CH_2O), 3.53 (2H, t, CH_2O), 3.49 (2H, t, CH_2O), 3.14 (2H, m, CH_2N), 2.27 (5 H, s, NH_2SO_2NH_3), 1.67 (2 H, s, B(9′, 12′)H); $\delta_{B\text{-}H}$ (from ^{1}H-{^{11}B} selective NMR experiments): 2.80 (1 H, s, B(10)H), 2.77 (2 H, s, B(4′, 7′)H), 2.66 (1 H, s, B(8′)H), 2.65 (2 H, s, B(4, 7)H), 2.58 (2 H, s, B(9, 12)H), 2.57 (1 H, s, B(10′)H), 1.63 (1 H, s, B(6′)H), 1.54 (2 H, s, B(5′, 11′)H), 1.45 (2 H, s, B(5, 11)H), 1.38 (1 H, s, B(6)H); ^{11}B NMR (128 MHz; CD_3CN; $Et_2O.BF_3$) δ_B/ppm: 23.67 (1 B, s, B8), 4.77 (1 B, d, J 140, B8′), −0.11 (1 B, d, J 140, B10), −2.72 (1 B, d, J 143, B10′), −5.05 (2 B, d, J 153, B4, 7), −7.62 (4 B, d, J 146, B9, 12, 9′, 12′), −9.07 (2 B, d, J 186, B4′, 7′), −17.49 (2 B, d, J 153, B5, 11), −20.49 (2 B, d, J 156, B5′, 11′), −22.36 (1 B, d, J 167, B6), −28.62 (1 B, d, J 168, B6′); ^{13}C NMR (100 MHz; CD_3CN; Me_4Si) δ_C/ppm: 72.42 (1 C, CH_2O), 70.45 (1 C, CH_2O), 69.19 (1 C, CH_2O), 53.98 (2 C, C$H_{carborane}$), 47.53 (2 C, C$H_{carborane}$), 43.98 (1 C, CH_2N). HRMS (ESI): m/z = 509.3311 (14%), 506.4205 (100%), calcd m/z = 509.3090 (14%), 506.3206 (100%), $[M]^-$; R_f = 0.18 (50% aqueous MeOH). Analysis Me_4N·**1**: found C 24.97, H 7.80, N 6.96. Calcd for $B_{18}C_{12}H_{44}O_4N_3SCo$: C 24.85, H, 7.65, N 7.24. HPLC purity assay: 95.9%.

8-(5-Sulfamido-1-oxapentyl)-3,3′-*commo*-bis(decahydro-1,2-dicarba-3-cobalta(III)-*closo*-dodecabor)ate (1-), (Na·2·H_2O). The starting ammonium derivative [8-(5-H_3N-C_5H_{10}-1-O)-$(1,2\text{-}C_2B_9H_{10})(1′,2′\text{-}C_2B_9H_{11})$-3,3′-Co(III)][40] was prepared according to a modified procedure by reacting the known cyclic tetrahydropyrronium derivative[39] with ammonia in THF. NMR and MS spectra were identical to those described in the literature. This ammonium derivative (102 mg, 0.24 mmol) was dissolved in 1,4-dioxane (5 mL). Solid sulfamide ($H_2NSO_2NH_2$, 225 mg, 2.34 mmol) followed by anhydrous Na_2CO_3 (225 mg, 1.63 mmol) was added under nitrogen, and the slurry was intensively stirred and heated under reflux for 3 h. The reaction course was followed by TLC (Silica gel, CH_3CN−CH_2Cl_2, 1:3) and MS (ESI$^-$). When the starting compound disappeared, the solvents were removed under reduced pressure. The resulting solid was treated with acetonitrile (5 mL), the slurry was filtered, and the filtrate was evaporated to dryness under reduced pressure. The solid residue was dissolved in ethyl acetate (10 mL) and treated in an extraction funnel with diluted HCl (3 M, 3 × 10 mL) and then washed with a saturated solution of NaCl (4 × 10 mL) until the aqueous phase reached neutral pH. The organic layer was separated, and volatiles were removed in a vacuum. The crude product was then dissolved in a mixture comprising CH_2Cl_2 and CH_3OH (10:3 bv, 26 mL). The solution was overlaid with hexanes (80 mL) and left to stand for 3 d. The orange semisolid product was separated by decantation and dried in a vacuum. Yield 98 mg (82%). ^{1}H NMR (CD_3CN, Me_4Si) δ_H/ppm: 4.10 (2 H, s, C$H_{carborane}$), 3.98 (2 H, s, C$H_{carborane}$), 3.51 (2 H, t, CH_2O), 2.92 (2 H, m, CH_2N), 2.21 (4 H, s, H_2NSO_2NH_2), 1.62 (2 H, m, CH_2), 1.43 (2 H, m, CH_2), 1.25 (2 H, m, CH_2). $\delta_{B\text{-}H}$ (from ^{1}H-{^{11}B} selective NMR experiments): 2.82 (1 H, s, B(10)H), 2.78 (1 H, s, B(8′)H), 2.65 (2 H, s, B(9′, 12′)H), 2.61 (2 H, s, B(9, 12)H), 2.58 (1 H, s, B(10′)H), 1.82 (2 H, s, B(4, 7)H), 1.70 (2 H, s, B(4′, 7′)H), 1.66 (1 H, s, B(6′)H); 1.55 (2 H, s, B(5′, 11′)H), 1.48 (2H, s, B(5, 11)H), 1.41 (1 H, s, B(6)H). ^{11}B NMR (CD_3CN; $Et_2O.BF_3$) δ_B/ppm: 23.87 (1 B, s, B8), 5.06 (1 B, d, J 140, B8′), −0.29 (1 B, d, J 140, B10), −2.88 (1 B, d, J 150, B10′), −2.79 (2 B, d, J 134, B9, 12), −5.12 (4 B, d, J 147, B4, 7, 9′, 12′), −6.31 (2 B, d, J 192, B4′, 7′), −7.48 (2 B, d, J 150, B5, 11), −17.51 (2 B, d, J 156, B5′, 11′), −20.37 (1 B, d, J 173, B6), −22.29 (1 B, d, J 174, B6′), −28.81 (1B, d, J 143, B6); ^{13}C {^{1}H} NMR (CD_3CN; Me_4Si) δ_C/ppm: 69.31 (1 C, CH_2O), 53.45 (1 C, CH_2N), 47.43 (2 C, C$H_{carborane}$), 40.93 (2 C, C$H_{carborane}$), 31.22 (1 C, CH_2), 26.94 (1 C, CH_2), 23.30 (1 C, CH_2). HRMS (ESI) m/z = 507.3315 (10%), 504.4224 (100%), calcd m/z = 507.3271 (14%), 504.3414 (100%) $[M]^-$; R_f = 0.19 (50% aqueous MeOH). Analysis Me_4N.**2**: found C 26.68, H 7.67, N 7.45. Calcd for $B_{18}C_{13}H_{46}O_3N_3SCo$: C, 27.01; H, 8.02, N 7.27. HPLC purity assay: >97.5%.

8-Sulfamidomethyl-8′-methoxy-3,3′-*commo*-bis(1,2-dicarba-3-cobalta(III)-*closo*-dodecabor)ate (1-), Sodium Salt (Na·3). The starting electroneutral bridged derivative [μ-8-CH_2-8′-CH_3O-$(1,2\text{-}C_2B_9H_{10})_2$-3,3′-Co(III)][41] (200 mg, 0.5 mmol) was dissolved in DME (7 mL). Then, sulfamide ($H_2NSO_2NH_2$, 157 mg, 1.6 mmol) was added under nitrogen, and the reaction mixture was stirred at room temperature for 7 days. The reaction course was monitored periodically by TLC and MS (ESI$^-$), and the stirring was stopped when the starting compound disappeared. The reaction was then quenched by evaporation of the solvent under reduced pressure. The resulting orange solid was treated with 50 mL of CH_2Cl_2, and the slurry was filtered through a glass filter. The filtrate was shaken with 30 mL of diluted HCl (3 M). The orange precipitate containing crude zwitterionic product was separated by filtration and then dissolved in CH_2Cl_2 (10 mL), to which CH_3OH was added (150 μL). The resulting orange solution was filtered, layered with hexanes (60 mL), and left to crystallize for 3 days. Pure crystalline product was obtained after filtration and drying in vacuum. Yield of Na·**3**·2H_2O 141 mg (52%). ^{1}H NMR (400 MHz; CD_3CN, Me_4Si) δ_H/ppm: 3.96 (2 H, s, 2 CH carborane), 3.92 (2 H, s, 2 CH carborane), 3.46 (3H, s, CH_3O), 3.23 (2 H, t, SO_2NH_2), 2.60 (1 H, t, NH), 1.25 (2 H, d, CH_2NH). $\delta_{B\text{-}H}$ (from ^{1}H-{^{11}B} selective NMR experiments): 2.92 (1 H, s, B(10)H), 2.91 (2 H, s, B(4′, 7′)H), 2.77 (2 H, s, B(4, 7)H), 2.64 (1 H, s, B(10′)H), 2.18 (2 H, s, B(9′, 12′)H), 1.94 (2 H, s, B(9, 12)H), 1.61 (1 H, s, B(6)H), 1.57 (2 H, s, B(5′, 11′)H), 1.54 (2H, s, B(5, 11)H), 1.43 (1 H, s, B(6′)H). ^{11}B NMR (128 MHz; CD_3CN; $Et_2O.BF_3$) δ_B/ppm: 25.46 (1 B, s, B8′), 9.22 (1 B, s, B8), 0.87 (1 B, d, J 143, B10), −2.13 (1 B, d, J 143, B10′), −4.58 (2 B, d, J 140, B9, 12), −6.29 (4 B, d, J 137, B4, 7, 9′, 12′), −7.74 (2 B, d, J 186, B4′, 7′), −18.30 (2 B, d, J 125, B5, 11), −18.92 (2 B, d, J 131, B5′, 11′), −22.65 (1 B, d, J 180, B6), −27.62 (1 B, d, J 153, B6′). ^{13}C {^{1}H} NMR (100 MHz; CD_3CN; Me_4Si) δ_C/ppm: 57.84 (1 C, CH_2), 52.58 (2 C, C$H_{carborane}$), 49.12 (2 C, C$H_{carborane}$), 14.58 (1 C, q, CH_3). HRMS (ESI): m/z = 465.2828 (10%), 462.2804 (100%), calcd m/z = 465.2828 (14%) 462.2942 (100%), $[M]^-$; R_f = 0.14 (50% aqueous MeOH). Analysis Me_4N·**3**: found C 22.65, H 8.10; N 7.57. Calcd for $B_{18}C_{10}H_{40}O_3N_3SCo$: C 22.41; H 7.52, N 7.84. HPLC purity assay: 98.5%..

8-Methyleneammonio-(*N*-2-sulfamidoethyl-)-8′-methoxy-3,3′-*commo*-bis(decahydro-1,2-dicarba-3-cobalta(III)-*closo*-dodecabor)ate (4). For the synthesis of the corresponding zwitterionic amine intermediate $\mathbf{II}_4$ see Supporting Information and Scheme S2 therein. The ammonium derivative $\mathbf{II}_4$ (50 mg, 0.12 mmol) was dissolved in 1,4-dioxane (5 mL). Sulfamide (112 mg, 1.17 mmol) was added under nitrogen, and the resulting slurry was stirred and heated under reflux. The reaction course was followed by TLC (CH_3CN−CH_2Cl_2, 1:3) and MS. When the starting compound disappeared (2 h under reflux), the solvent was removed under reduced pressure. The dry solid was treated with 5 mL of acetonitrile, and the resulting slurry was filtered. Then, the solvent was evaporated under reduced pressure, and the resulting orange solid was dissolved in diethyl ether (10 mL) and shaken with diluted HCl (2 M, 4 × 10 mL). The organic layer was separated and evaporated under reduced

DOI: 10.1021/acs.jmedchem.9b00945
J. Med. Chem. 2019, 62, 9560−9575

pressure. The crude product was dissolved in a mixture containing 20 mL of CH_2Cl_2 and 2 mL of CH_3OH, and the solution was layered with hexanes (80 mL) and left to stand overnight. The solid product was decanted from the mother liquors and dried in a vacuum. Yield 38 mg (64%). $^1H\{^{11}B\}$ NMR (400 MHz; CD_3CN, Me_4Si) δ_H/ppm: 7.14 (2 H, br, t, NH_2), 5.21 (4 H, br, s, $CH_2NH_2SO_2NH_2$), 3.89 (2 H, s, $CH_{carborane}$), 3.84 (2 H, s, $CH_{carborane}$), 3.44 (3H, s, CH_3O), 3.27 (2H, q, CH_2NH_2), 3.13 (2H, p, CH_2NH_2). $\delta_{B\text{-}H}$ (from $^1H\text{-}\{^{11}B\}$ selective NMR experiments): 2.98 (2 H, t, B(8′)*H*), 2.83 (1 H, s, B(10)*H*), 2.82 (2 H, s, B(4′, 7′)*H*), 2.72 (2 H, s, B(4, 7)*H*), 2.61 (1 H, s, B(10′)*H*), 1.88 (2 H, s, B(9, 12)*H*), 1.76 (2 H, s, B(9′, 12′)*H*), 1.57 (1 H, s, B(6)*H*), 1.57 (2 H, s, B(5′, 11′)*H*), 1.54 (2H, s, B(5, 11)*H*), 1.41 (1 H, s, B(6′)*H*). ^{11}B NMR (128 MHz; CD_3CN; $Et_2O.BF_3$) δ_B/ppm: 26.70 (1 B, s, B8′), 9.98 (1 B, s, B8), −0.20 (1 B, d, *J* 146, B10), −2.48 (1 B, d, *J* 143, B10′), −5.29 (2 B, d, *J* 153, B9, 12), −6.52 (4 B, d, *J* 162, B4, 7, 9′, 12′), −8.16 (2 B, d, *J* 208, B4′, 7′), −18.18 (2 B, d, *J* 143, B5, 11), −19.05 (2 B, d, *J* 146, B5′, 11′), −23.29 (1 B, d, *J* 198, B6), −28.19 (1 B, d, *J* 183, B6′). ^{13}C NMR (100 MHz; CD_3CN; Me_4Si) δ_C/ppm: 58.15 (1 C, t, CH_2), 51.50 (2 C, d, $CH_{carborane}$), 50.32 (2 C, t, CH_2N), 48.42 (2 C, d, $CH_{carborane}$), 39.74 (1 C, q, CH_3). HRMS (ESI): 508.3288 (15%), 505.2596 (100%), calcd 508.3296 (15%) 505.3366 (100%) $[M - H]^-$; R_f = 0.12 (50% aqueous MeOH). Analysis **4**: found C 18.62, H 6.36; N 8.61. Calcd for $B_{18}C_8H_{34}O_3N_3SCo$: C, 18.99; H, 6.77, N 8.30. HPLC purity assay: >98%.

General Procedure Leading to 1-Sulfamidoalkyl-3,3′-*commo*-bis(1,2-dicarba-3-cobalta(III)-*closo*-dodecabor)ates (1$^-$) (Me_4N·5−7). The tetramethylammonium salts of starting amines of the general formulation $[(1\text{-}H_2N\text{-}(CH_2)_n\text{-}1,2\text{-}C_2B_9H_{10})(1',2'\text{-}C_2B_9H_{11})\text{-}3,3'\text{-}Co]Me_4N$ (n = 1 to 3) were prepared and characterized according to a previously described procedure.[43] The starting salts (0.50 mmol) were dissolved upon shaking in an ether−ethyl acetate mixture (3:1 bv, 50 mL) and washed with diluted HCl (3 M, 4 × 50 mL) and then water (30 mL). The organic layer was separated, evaporated to dryness on a rotary evaporator, and dried 2 h in a vacuum at room temperature and then for 6 h at 45 °C. Sulfamide (240 mg, 2.50 mmol) and anhydrous potassium carbonate (140 mg, 1.0 mmol) were dried separately for 10 h in a vacuum at room temperature and then poured into a flask containing the amine. 1,4-Dioxane (30 mL) was added through a rubber septum, and the reaction mixture was heated to 80 °C under stirring for 2 h and then under gentle reflux for 4−12 h. The course of the reaction was monitored by HPLC and MS, and the reaction was stopped when the starting compound had almost disappeared. After cooling, the solids were filtered out under nitrogen, washed with dioxane (4 × 5 mL), and discarded. The combined organic extracts were evaporated under reduced pressure, and the resulting solid residue was dissolved in an ether−ethyl acetate mixture (4:1 bv, 50 mL) and shaken with diluted HCl (1.5 M, 4 × 50 mL). The organic layer was separated, water (15 mL) was added, and the organic solvents were removed under reduced pressure. Partly solidified products were dissolved by addition of a small volume of MeOH. The crude products were precipitated by addition of an excess of an aqueous solution of Me_4NCl. The slurry was left to stand for ∼30 min, and the solids were separated by filtration or decantation, washed with water (2 × 5 mL), and dried in a vacuum. The orange residue was dissolved in a minimal volume of a CH_2Cl_2 and CH_3CN mixture (4:1 bv). This solution was injected onto a silica gel column (20 × 1.5 cm) and eluted with a CH_2Cl_2−CH_3CN solvent mixture with a gradually increasing acetonitrile content from 20% to 40% bv. The first collected fraction usually contained small amounts unreacted starting ammonium derivatives. Other fractions corresponding to pure product (according to HPLC and MS) were combined and evaporated under reduced pressure. The solid orange compound was dissolved in CH_2Cl_2 (25 mL) with addition of a few drops of acetone. The resulting solution was carefully layered with hexanes (40 mL) and left to crystallize for 3 days. A semicrystalline product separated, which was decanted, washed with a small amount of hexanes, and dried 6 h under reduced pressure at 50 °C.

1-Sulfamidomethyl-3,3′-*commo*-bis(1,2-dicarba-3-cobalta-(III)-*closo*-dodecabor)ate (1-) (Na·5 and Me_4N·5). Reaction time 20 h. Yield of Na**5**·$3H_2O$: 115 mg (39%). Me_4N·**5** ^1H NMR (400 MHz; CD_3CN, Me_4Si) δ_H/ppm: 5,233 (2H, s, $NHSO_2NH_2$), 5,161 (1H, br, t, CH_2NHSO_2), 4.011, 3.933, 3.911 (3H, 3 br, s, $CH_{carborane}$), 3.857 (2H, d, *J* = 6.8 Hz, -CH_2-NH), 3.44 (12H, Me_4N^+). $\delta_{B\text{-}H}$ (from $^1H\text{-}\{^{11}B\}$ selective NMR experiments): 3.557, 3.391 (2H, 2s, B(8,8′)*H*), 2.903 (2H, s, B(10,10′)*H*); 2.709, 2.652, 2.585, 1.85 (8H, s, B(4,7,4′,7′,9,12, 9′,12′)*H*); 2.084 (8H, s, H_2O), 1,624 (1H, s, B(6)*H*), 1.624 (1H, s, B(6′)*H*), 1.587 (1H, s, B(5)*H*), 1.554 (1H, s, B(11)*H*), 1.497 (2H, s, B(5′,11′)*H*). ^{11}B NMR (128 MHz; CD_3CN; Et_2O,BF_3) δ_B/ppm: 6,24 (2B, d, *J* = 153 Hz, B8,8′), 0.988 (2B, d, *J* = 143 Hz, B10,10′), −6.29, −6.86 (8B, 4d, overlap, B4,7,4′,7′,9,12, 9′,12′), −14.35, −16.97 (2B, 2d, *J* = 152 Hz, overlap, B5,11), −17.59 (2B, d, *J* = 159 Hz, B5′,11′), −20.53 (1B, d, *J* = 171 Hz, B6), −22.72 (1B, d, *J* = 171 Hz, B6′). ^{13}C NMR (100 MHz; CD_3CN; Me_4Si) δ_C/ppm: 66,47 (1 C, s, $C_{carborane}$), 54.88 (1 C, d, $CH_{carborane}$), 52.72 (1 C, $CH_{carborane}$), 52.04 (1 C, $CH_{carborane}$), 51.05 (1 C, m, CH_2NH); R_f = 0.17 (50% aqueous MeOH); mp 235−240 °C. HRMS (ESI$^-$) 432.3034 (100%), 435.30065 (14%), calcd: 432.2836 (100%) 435.2722 (14%), $[M]^-$. Analysis Me_4N·**5**: found C 21.68, H 7.46; N 8.21. Calcd for $B_{18}C_9H_{38}O_2N_3SCo$: C, 21.36; H, 7.57, N 8.30. HPLC purity assay: 99.1%.

1-Sulfamidoethyl-3,3′-*commo*-bis(1,2-dicarba-3-cobalta-(III)-*closo*-dodecabor)ate (1-) (Na·6 and Me_4N·6). Yield of Na**6**·$3H_2O$: 185 mg (66%). Me_4N·**6** ^1H NMR (400 MHz; acetone-d_6, Me_4Si) δ_H/ppm, 5.38 (2H, br s, $NHSO_2NH_2$), 5.22 (1H, br, t, CH_2NHSO_2), 4.12, 3.81, 3.75 (3H, 3 br s, $CH_{carborane}$), 3.22 (12H, s, Me_4N^+), 2.98 (2H, m, *J* = 6,4 Hz, -CH_2-NH), 2.56 (2H, 2m, -CH_2-CH_2-NH). $\delta_{B\text{-}H}$ (from $^1H\text{-}\{^{11}B\}$ selective NMR experiments): 3.013, 3.785, 3.295 (2H, 2s, B(8,8′)*H*), 3.295, 2.934 (2H, s, B(10,10′)*H*); 2.841 (2H, s, B(10,10′)*H*), 2.645, 2.494, 1.910, 1.844 (8H, 4s, B(4,7,4′,7′,9,12, 9′,12′)*H*); 1.911, 1.875, 1.847, 1.659, (4H, 4s, B(5, 11,5′,11′)*H*), 1.783 1.788 (2H, 2s, B(6, 6′)*H*). ^{11}B NMR (128 MHz; acetone-d_6; Et_2O,BF_3) δ_B/ppm: 6.53 (2B, d, *J* = 146 Hz, B8,8′), 0.85 (2B, d, *J* = 140 Hz, B10,10′), −5.33, −6.05, −6.89 (8B, 4d, overlap, B4,7,4′,7′,9,12, 9′,12′), −15.34, −16.23 (2B, 2d, *J* = 161 Hz, B5,11), −17.62 (2B, d, *J* = 171 Hz, B5′,11′), −19.41 (1B, d, overlap, B6), −22.81 (1B, d, *J* = 180 Hz, B6′). $^{13}C\{^1H\}$ NMR (100 MHz; acetone-d_6; Me_4Si) δ_C/ppm: 67.0 (1 C, $C_{carborane}$), 57.95 (Me_4N^+) 54.30 (1 C, $CH_{carborane}$), 51.87 (1 C, $CH_{carborane}$), 49.79 (1 C, $CH_{carborane}$), 44.85 (1 C, CH_2NH), 40.00 (1 C, CH_2-CH_2NH). MS (ESI$^-$) 446.50 (100%), 449.33 (14%), calcd 446.29 (100%), 449.29 (14%) $[M]^-$; R_f = 0.34 (50% aqueous MeOH); Me_4N·**6** mp 220−223 °C. Analysis Me_4N·**6**: found C 23.47, H 7.78. Calcd for $B_{18}C_{10}H_{40}O_2N_3SCo$: C, 23.10; H, 7.75. HPLC purity assay: 100%. This compound was prepared repeatedly for in vivo tests starting from 3 mM of the respective amine, purified as Me_4N·**6** and then converted to the corresponding Na^+ salt by methathesis (see Supporting Information).

1-Sulfamidopropyl-3,3′-*commo*-bis(1,2-dicarba-3-cobalta-(III)-*closo*-dodecabor)ate (1-) (Me_4N·7). Yield of Na7·$3H_2O$: 165 mg (45%). ^1H NMR (400 MHz; acetone-d_6, Me_4Si) δ_H/ppm, 5.82 (2H, s, $NHSO_2NH_2$), 5.73 (1H, br, t, CH_2NHSO_2), 4.028, 3.709, 3.653 (3H, 3 br. s, $CH_{carborane}$), 3.038 (2H, m, *J* = 6,4 Hz, -CH_2-NH), 2.845 and 2.781 (2H, 2m, -CH_2-CH_2-NH), 2.877 (2H, H_2O), 1.82 (2H, 2m, C-CH_2). $\delta_{B\text{-}H}$ (from $^1H\text{-}\{^{11}B\}$ selective NMR experiments): 2.841 (2H, s, B(10,10′)*H*), 3.557, 3.391 (2H, 2s, B(8,8′)*H*), 3,597 (2H, s, B(10,10′)*H*); 2.633, 2.634, 1.958, 1.904 (8H, 4s, B(4,7,4′,7′,9,12, 9′,12′)*H*); 1.714, 1.659, 1.531 (4H, s, B(5, 11,5′,11′)*H*), 1.624 1.629 (2H, 2s, B(6, 6′)*H*). ^{11}B NMR (128 MHz; acetone-d_6; Et_2O,BF_3) δ_B/ppm: 6.46 (2B, d, *J* = 141 Hz, B8,8′), 0.56 (2B, d, *J* = 143 Hz, B10,10′), −6.12, −7.022 (8B, 4d, overlap, B4,7,4′,7′,9,12, 9′,12′), −14.94, −16.37 (2B, 2d, *J* = 177 Hz, B5,11), −17.84 (2B, d, *J* = 180 Hz,, B5′,11′), −19.25 (1B, d, *J* = 200 Hz, B6), −22.98 (1B, d, *J* = 179 Hz, B6′). $^{13}C\{^1H\}$ NMR (100 MHz; acetone-d_6; Me_4Si) δ_C/ppm: 69,53 (1 C, $C_{carborane}$), 58.03 (1 C, $C_{carborane}$), 56.4 (4C, Me_4N^+), 54.13 (1 C, $C_{carborane}$), 51.63 (1 C, $C_{carborane}$), 43.72 (1 C, CH_2NH), 38.12 (1 C, CH_2-CH_2NH), 31.55 (1C, C−CH_2). MS (ESI$^-$): 460.33 (100%), 463.33 (12%), calcd 460.30 (100%), 463.30 (14%) $[M]^-$; R_f = 0.26 (50% aqueous MeOH); mp 185−189 °C.

DOI: 10.1021/acs.jmedchem.9b00945
J. Med. Chem. 2019, 62, 9560−9575

Analysis $Me_4N(7)$: found C 24.46, H 7.73, N, 7.83. Calcd for $B_{18}C_{11}H_{42}O_2N_3SCo$: C, 24.74; H, 7.93, N, 7.87. HPLC purity assay: 100%.

1,1′-(Disulfamidoethyl)-3,3′-*commo*-bis(1,2-dicarba-3-cobalta(III)-*closo*-dodecabor)ate (1-) (Na·8 and Me_4N·8). The *anti*-isomer of dihydroxyethyl derivative $\mathbf{I_8}$ was prepared in 99.6% purity (according to HPLC) by 5-fold crystallization of a mixture of trimethylammonium salts of the *syn*- and *anti*-isomers prepared using previously reported conditions[43] from CH_2Cl_2 and hexanes. The *anti*-isomer crystallizes preferentially. The tetramethylammonium salt of the starting amine $[(1,1'\text{-}(H_2N\text{-}C_2H_4)_2\text{-}1,2\text{-}C_2B_9H_{10})_2\text{-}3,3'\text{-}Co]Me_4N$ $[Me_4N(\mathbf{III_8})]$ was prepared by esterification of the intermediate $\mathbf{I_8}$ and reaction of the resulting methylsulfonyl ester $[Me_4N(\mathbf{II_8})]$ with ammonia;[43] see Scheme S4 in the Supporting Information. The amine intermediate $Me_4N(\mathbf{III_8})$ (1.21 g, 2.50 mmol) in Et_2O−ethyl acetate (4:1 bv, 50 mL) was shaken with diluted HCl (3 M, 4 × 25 mL). The organic layer was separated and washed with water (2 × 20 mL). The organic solvents were removed in a vacuum, and the residue was dried for 2 h in ambient temperature and 6 h at 50 °C. The red solid was then reacted with sulfamide (2.4 g, 25 mmol) and anhydrous potassium carbonate (7.0 g, 25 mmol) in dioxane (75 mL) under reflux for 24 h, similar to the procedure described above for monosubstituted compounds. Product isolation was similar to that described for $Me_4N(\mathbf{5}-\mathbf{7})$; however, the chromatography and crystallization were repeated twice to remove a side product that exhibited m/z = 472.42 in its mass spectrum and a singlet in ^{11}B NMR. This side product was tentatively characterized by MS and NMR spectroscopy as a compound containing one sulfamidoethyl group and an ethylene bridge between positions C(1) and B(8′) of the cage; details are not shown. Yield of Me_4N·**8** (*anti*-$\mathbf{8}^-$): 980 mg (61%), red solid. This salt was transferred to the sodium form by methathesis (see Supporting Information). Na·(*anti*-$\mathbf{8}^-$): ^1H NMR δ_H(400 MHz; acetone-d_6): 5.27 (4H, s, $NHSO_2NH_2$), 5.15 (2H, br, t, CH_2NHSO_2), 3.69 (2H, s, *CH* carborane), 3.25, (4H, m, CH_2N), 2.71 (2H, br m, J = 10.8, C-CH_2CH_2), 2.38 (2H, br s, C-CH_2CH_2). $\delta_{B\text{-}H}$ (from ^1H-{^{11}B} selective NMR experiments) 4.07 (2H, s, B(8, 8′)*H*), 2.89 (2H, s, B(10, 10′)*H*), 2.18 (2H, s, B(9, 9′)*H*), 2.43 (2H, s, B(4, 4′)*H*), 2.96 (2H, s, B(7, 7′)*H*), 1.78 (2H, s, B(12, 12′)*H*), 1.78 (2H, s, B(5, 5′)*H*), 1.72 (2H, s, B(11, 11′)*H*), 1.70 (2H, s, B(6, 6′)*H*). ^{11}B NMR δ_B(128 MHz; acetone-d_6; $Et_2O{\cdot}BF_3$): 8.31 (2B, br d, J = 149 Hz, B8, 8′), −0.07 (2B, br d, J 143, B10, 10′), −3.64 (2B, d, J 143, B9, 9′), −4.88 (2B, d, overlap, B4, 4′), −6.54 (2B, d, J 122, B7, 7′) −8.50 (2B, d, J 140, B12, 12′), −14.3, −15.92 (2B, d, J 165, B5, 5′, B11, 11′), −19.77 (2B, d, J 165, B6, B6′). $^{13}C\{^1H\}$ NMR δ_C (100 MHz; acetone-d_6): 68.45 (2C, $C_{carborane}$), 59.1 (2C, *CH* carborane), 45.08 (2C, (CH_2NH), 40.6 (2C, C-CH_2). MS (ESI) m/z = 571.36 (M^-, 10%), 568.36 (100%), calcd 571.31 (16%) and 568.31(100%) $[M]^-$; Me_4N(*anti*-$\mathbf{8}^-$): R_f = 0.58 (50% aqueous MeOH); mp 220−225 °C. Analysis Me_4N(*anti*-**8**)·H_2O: found C 21.51, H, 7.41, N 10.34. Calcd for $B_{18}C_{12}H_{48}O_5N_5S_2Co$: C, 21.83; H, 7.33; N, 10.61. This compound was prepared repeatedly for in vivo tests starting from 3 mM of the respective amine and converted to the corresponding sodium salt. HPLC purity assay: 97.8%.

1,2′-(Disulfamipropyl)-3,3′-*commo*-bis(1,2-dicarba-3-cobalta(III)-*closo*-dodecabor)ate (1-) (Me_4N·9). For synthesis of intermediate compounds ($\mathbf{I_9}$, $\mathbf{II_9}$, and $\mathbf{III_9}$) with terminal -OH, -OMs, and -NH_2 groups, see Supporting Information and Scheme S5 therein. The amine intermediate $\mathbf{III_9}$ of formula $[(1,2'\text{-}(H_2N\text{-}C_3H_6)_2\text{-}1,2\text{-}C_2B_9H_{10})_2\text{-}3,3'\text{-}Co]Me_4N$ (65 mg, 0.125 mmol) was reacted with sulfamide (120 mg, 1.25 mmol) and anhydrous potassium carbonate (138 mg, 1.25 mmol) in dioxane (15 mL) under reflux for 24 h (the same procedure used for synthesis of disulfamide $\mathbf{8}^-$). The product was isolated as described above for $\mathbf{8}^-$; however, the chromatography and crystallization were repeated twice to remove the monosulfamide and other derivatives present as impurities after reaction. Yield of Me_4N·**9**: 40 mg (47%), orange-red solid. ^1H NMR δ_H (400 MHz; acetone-d_6): 5.89 (4H, s, NH_2), 5.78 (2H, t, J = 5.8 Hz, *NH*), 4.06 (2H, br s, carborane *CH*), 3.46 (12H, s, $(CH_3)_4N$), 3.04 (4H, t, J = 5.6 Hz, $CCH_2CH_2CH_2NH$), 2.15 (4H, m, $CCH_2CH_2CH_2$), 1.84 (2H, m, $CCH_2CH_2CH_2$), 1.58 (2H, m, $CCH_2CH_2CH_2$). ^{11}B NMR δ_B (128 MHz; acetone-d_6; $Et_2O.BF_3$): 7.22 (2B, d, J = 113 Hz, B8, 8′), −0.15 (2B, d, J = 140 Hz, B10, 10′), −5.52 (6B, d, J = 110 Hz, B4, 4′, 9, 9′, 12, 12′), −7.71 (2B, d, J = 140 Hz, B7, 7′), −14.33 (1B, d, *overlap* B5), −15.63 (3B, d, *overlap*, B5′, 11, 11′), −18.41 (2B, d, J = 108 Hz, B6, 6′). ^{13}C NMR δ_C (100 MHz; acetone-d_6): 56.00 (2C, *carborane* C), 55.29 (4C, $(CH_3)_4N$), 43.97 (2C, *carborane* CH), 31.91 (2C, $CCH_2CH_2CH_2NH$), 27.75 (2C, $CCH_2CH_2CH_2$), 14.34 (2C, $CCH_2CH_2CH_2$); R_f = 0.53 (50% aqueous MeOH); mp 207 °C; MS (ESI): m/z = 597.61 (19%), 594.59 (100%), calcd 597.32 (19%) and 594.32 (19%). Analysis found: C, 25.32; H, 7.71, N, 10.36. Calcd for $B_{18}C_{14}H_{50}N_5O_4S_2Co$: C, 25.09; H, 7.52, N, 10.45. HPLC purity assay: 100%.

CA Inhibition Assay. Recombinant CAII expressed in *E. coli* and the extracellular part of CAIX comprising residues 38−391 (PG and CA domains) expressed in HEK 293 cells were used in inhibition assays. Protein cloning, expression, and purification procedures are described in Supporting Information. CA-catalyzed CO_2 hydration activity was assayed by an Applied Photophysics stopped-flow instrument. The starting CO_2 concentration was 8.5 mM. To stabilize CAIX, 0.0025% dodecyl-β-D-maltopyranosid (DDM, Anatrace) was included in the reaction mixture. K_i' values were obtained from dose−response curves recorded for at least six different concentrations of the test compound by nonlinear least-squares methods using an Excel spreadsheet fitting the Williams−Morrison equation.[76] The K_i values were then derived using the Cheng−Prusoff equation.

Protein Crystallography. For X-ray studies, CAII with A65S, N67Q, E69T, I91L, F130V, K169A, and L203A amino acid substitutions was used as a CAIX mimic.[51] The enzyme was prepared in *E. coli* and purified as described in Supporting Information. Complexes of the CAIX mimic with $\mathbf{5}^-$, $\mathbf{6}^-$, and $\mathbf{7}^-$ were crystallized, and diffraction data at 100 K were collected using the BL14.1 beamline operated by the Helmholtz-Zentrum Berlin (HZB) at the BESSY II electron storage ring (Berlin-Adlershof, Germany).[64] The XDS suite of programs[65,66] was used to process diffraction data. The crystal structure of the CAIX mimic in complex with $\mathbf{5}^-$ and $\mathbf{7}^-$ was determined by difference Fourier technique, and the structure of the complex with $\mathbf{6}^-$ was solved by molecular replacement with the MolRep program. The CAII structure (PDB entry 3PO6 [67]) was used as a model, and structures were refined using data to 1.1 Å resolution. The crystallization procedure, structure refinement, and analyses are described in Supporting Information. Atomic coordinates and structure factors were deposited in the PDB under accession codes 5OGP and 5OGN. Data collection and structure refinement statistics are summarized in Supporting Information, Table S2.

Cell Lines. Canine kidney MDCK cells not expressing CAIX (MDCK-neo) and stably transfected to overexpress CAIX (MDCK-CAIX) were kindly provided by Prof. Sylvia Pastoreková, Slovak Academy of Sciences, Bratislava, Slovakia, and maintained as previously described.[68] The luciferase-expressing mouse breast cancer 4T1-12B-luc cell line was provided by Prof. Danuta Radzioch, The Research Institute of the McGill University Health Centre, Montreal, Canada, and maintained as previously described.[69] Multidrug resistance protein 1 (MDR1)-expressing MDCK (MDCK-MDR1), HCT116, HT-29, Caco-2, CCRF-CEM, K562, MRC-5, HeLa, BJ, and A549 cell lines were obtained from ATCC (Middlesex, U.K.) and maintained according to recommendations. Multidrug-resistant sublines (CEM-DNR, K562-TAX) expressing the LRP and P-glycoprotein transporter proteins involved in tumor resistance were derived and cultured as previously described.[70] All cell lines were tested for mycoplasma contamination and authenticated weekly or monthly.

Cytotoxicity Assay. The cytotoxicity and/or antiproliferative activity of sodium salts of all compounds was tested under in vitro conditions using a 3-day tetrazolium salt reduction assay in 384-well format on a robotic high-throughput screening platform (HighResBio, Boston, MA). The IC_{50} values were calculated from the appropriate dose−response curves (see Supporting Information for details).

MCS Generation and Drug Treatment. Multicellular spheroids (MSCs) of HCT116 and HT-29 cells were generated as previously described.[71] Three-day-old MCSs were treated with $\mathbf{6}^-$ and $\mathbf{8}^-$, in the

DOI: 10.1021/acs.jmedchem.9b00945
J. Med. Chem. 2019, 62, 9560−9575

form of Na^+ salts, or U-104 at concentrations ranging from 333 μM to 0.1 μM for 3−7 days and imaged in a high-content imaging system (Yokogawa Electric Corporation, Tokyo, Japan) as previously described.[71] The images were analyzed using an in-house algorithm, and the effect of the compound on MCS size was calculated as a percentage of untreated controls.[71] The IC_{50} values of compounds were determined from the respective dose−response curves using GraphPad Prism software (version 7; GraphPad Prism, San Diego, CA).

MCS Immunoblot and Whole-Mount Immunostaining. Ten-day-old MCSs were treated with 1× and 0.5× IC_{50} concentrations of sodium salts of $\mathbf{6}^-$ and $\mathbf{8}^-$ in MCSs (Figure S2) for 3 days. For Western blot, 30−40 MCSs were collected, dispersed into single cells using Accutase cell detachment solution (Sigma-Aldrich, Prague, Czech Republic), and lysed in RIPA cell lysis buffer containing protease inhibitors by sonication on ice. Protein lysates were electrophoresed following a standard gel electrophoresis protocol. Primary antibodies used in the study included mouse monoclonal M75 anti-CAIX (BioScience Slovakia s.r.o., Bratislava, Slovakia; 3 μg/mL dilution) and mouse monoclonal anti-β-actin (Sigma-Aldrich; 1:4000 dilution) antibodies. Immunoblots were developed using anti-mouse Alexa Fluor 488-labeled secondary antibody (Thermo Fisher Scientific, Inc., Waltham, MA; 1:2000 dilution).

MCSs were processed for whole-mount immunostaining using M75 (BioScience Slovakia s.r.o.; 5 μg/mL dilution) and anti-mouse Alexa Fluor 488-labeled secondary antibody (1:1000 dilution) as described in the literature.[72] Prior to imaging, MCSs were counterstained with Hoechst 33342 nucleic acid stain (Molecular Probes, Eugene, OR) for 2−3 h. Immunostained MCSs were washed 2× with PBS and embedded into a 1% low-melting agarose cooled to 40 °C. MCSs were loaded into glass capillary tubes (Carl Zeiss Microscopy GmbH, Jena, Germany) and imaged in a Lightsheet Z.1 microscope (Carl Zeiss) with 20×/1.0 detection optics and two-sided 10×/0.2 illumination optics as previously described.[73] Images were processed using ZEN 2012 Black Edition imaging software (Carl Zeiss).

Hypoxia Treatment and Immunofluorescence in 2D Culture. HT-29 cells were treated with $\mathbf{6}^-$ and $\mathbf{8}^-$ in the form of sodium salts for different time intervals under hypoxic conditions in a Heracell 150i humidified incubator (Thermo Fisher Scientific) set to 1% O_2, 94% N_2, and 5% CO_2 at 37 °C. Following drug treatment, cells were fixed in 3.7% (v/v) formaldehyde and incubated in blocking buffer containing 2% bovine serum albumin, 1% fetal bovine serum (FBS; Gibco, Thermo Fisher Scientific), and 0.3% Triton X-100 dissolved in PBS. Cells were then stained with mouse anti-CAIX M75 antibody (BioScience Slovakia s.r.o.; 3 μg/mL) followed by incubation with anti-mouse Alexa Fluor 488-labeled secondary antibody (Thermo Fisher Scientific; 1:2000 dilution). Cells were mounted onto slides using ProLong Gold Antifade Mountant with DAPI nuclear stain (Thermo Fisher Scientific) and imaged in a spinning disk confocal microscope (Carl Zeiss) using an oil-immersion 63× objective.

Doxorubicin Penetration Studies. To determine the penetration of DOX, a prototypical fluorescent anticancer drug, in the presence of sodium salts of $\mathbf{6}^-$, $\mathbf{8}^-$, and cobalt bis(dicarbollide), time-lapse images of MCSs were acquired with a Lightsheet Z.1 microscope (Carl Zeiss). Equal-sized 10-day-old MCSs of HT-29 cells were collected and washed in PBS and transferred into an Eppendorf tube with mounting medium consisting of 0.2% low-melting agarose (Sigma-Aldrich) in phenol red-free EMEM medium supplemented with 5% FBS (Gibco), 2 mM L-glutamine, and 10 mM HEPES (Thermo Fischer Scientific). Prior to transferring the MCSs, the mounting medium was spiked with DOX (25 μM) and 3× day 7-IC_{50} concentration of either $\mathbf{6}^-$ (430 μM) or $\mathbf{8}^-$ (180 μM). MCSs were treated with sodium cobalt bis(dicarbollide) to a final concentration of 430 μM, a concentration equivalent to that of $\mathbf{6}^-$. MCSs were then drawn into an optically clear, 3 cm long fluorinated ethylene propylene (FEP; Bohlender GmbH, Grünsfeld, Germany) tube using a metal plunger (Carl Zeiss). One end of the FEP tube was fitted with a 1.5 mm (inner diameter) glass capillary tube (Zeiss), and the other end was plugged with 2% low-melting agarose. The FEP tube was then inserted into a sample holder and placed in a specimen chamber containing phenol-red free EMEM medium supplemented with 10 mM HEPES. A 3D stack of 25 images at 10 μm intervals was captured from two directions every 10 min for 2−3 h using 20×/1.0 detection optics and 10×/0.2 illumination optics. DOX was excited with a 488 nm laser, and the emission was collected using a 575−615 band-pass emission filter. Images were processed using ZEN 2012 imaging software (Carl Zeiss), and DOX fluorescence intensity at 50 μm z-plane height was measured by normalizing the DOX signal to the penetration area as described by Gong et al.[74] MCSs in the specimen chamber were maintained at 37 °C and 5% CO_2 during the entire imaging.

Raman Spectroscopy. HT-29 cells were grown under hypoxic conditions on CaF_2 substrates (polished Raman grade CaF_2 windows, 4 mm × 4 mm × 1 mm; Crystran, Poole, Dorse, U.K.) in DMEM with 10% FBS for 3 days until they reached 60% confluency. Prior to drug treatment, high serum medium was replaced with DMEM containing 2% Xerum free supplement (TNCBio, Eindhoven, The Netherlands) to diminish cobaltacarborane interactions with serum proteins. Treated cells were incubated in hypoxic conditions for 12 h, fixed in 1% formaldehyde, washed with PBS, and processed for Raman spectroscopy as described in Supporting Information.

In Vitro Pharmacology. Compounds $\mathbf{6}^-$ and $\mathbf{8}^-$ in the form of Na^+ salts were assayed in vitro for human plasma and liver microsomal stability and subjected to an artificial membrane permeability assay (PAMPA) and cellular permeability models of gastrointestinal resorption blood−brain barrier using Caco-2 and MDR1-MCDK cells as previously described.[75] Samples were analyzed in an Agilent RapidFire 300 high-throughput mass spectrometry system (RF-MS; Agilent, Wakefield, MA) with subsequent detection in a Qtrap 5500 mass spectrometer (AB Sciex, Concord, Canada). See Supporting Information for details.

In Vivo Pharmacokinetics. Compounds $\mathbf{6}^-$ and $\mathbf{8}^-$ in the form of Na^+ salts were administered intraperitoneally to female NMRI mice at the maximum tolerated dose (MTD; 125 mg/kg for both compounds). Animals were sacrificed under anesthesia by bleeding from the brachial plexus after 0.5, 1, 3, 6, 9, 12, 24, and 36 h (3 mice per group). The blood was collected on ice and processed for serum separation within 60 min after sampling. The serum samples were evaporated to dryness on a vacuum centrifuge (72 h, 50 °C) and subsequently analyzed. Residues were precipitated by addition of 225 μL of acetonitrile followed by 25 μL of 10% SDS (w/w in water), then vortexed for 5 min and centrifuged for 5 min at 14 000 rpm at room temperature.

The boron and cobalt content in serum after compound administration was determined using a SPECTRO ARCOS ICP optical emission spectrometer with radial plasma observation (Spectro Analytical Instruments, Kleve, Germany). The SPECTRO ARCOS features a Paschen-Runge spectrometer that enables simultaneous spectral analysis in the wavelength range from 130 to 770 nm. For sample introduction, an ETV 4000c system electrothermal vaporization device (Spectral Systems, Fürstenfeldbruck, Germany) was used. The ETV method involves placing a few milligrams of sample material into a graphite furnace, where the material is vaporized, halogenated using a modifier gas, transferred to the ICP-OES, and introduced into the plasma as a dry aerosol. A special software module enables processing of the transient signal of the tracked element wavelengths (three lines for each element) from ICP synchronized with the ETV-temperature program. The detection limit of the method was 0.010 ppm for boron and 0.006 ppm for cobalt (typical RSD $\leq$ 3%, three replicates per measurement).

Mouse Xenografts. The antitumor activities of sodium salts of $\mathbf{6}^-$, $\mathbf{8}^-$, and the reference CAIX inhibitor U-104[56] were tested in female SCID mice xenografted with HT-29 cells and female Balb/c mice orthoptically transplanted with syngenic 4T1 breast cancer cells. See Supporting Information for details. All animal procedures were approved by the Animal Ethics Committee of the Faculty of Medicine and Dentistry, Palacký University Olomouc, Czech Republic.

DOI: 10.1021/acs.jmedchem.9b00945
J. Med. Chem. 2019, 62, 9560−9575

Statistical Analysis. Considering biological experiments, statistical analyses were performed using GraphPad Prism software (GraphPad Prism), and differences were considered significant at $p < 0.05$.

■ ASSOCIATED CONTENT

Supporting Information

The Supporting Information is available free of charge on the ACS Publications website at DOI: 10.1021/acs.jmedchem.9b00945.

Additional details on the synthetic procedures and schemes for synthesis of target compounds $\mathbf{1}^-$ to $\mathbf{9}^-$, inclusive starting amines; experimental details for the protein purification and CA inhibition assay protein crystallization; structure determination, refinement and analysis; Raman spectroscopy; in vitro and in vivo pharmacology and in vivo antitumor activity studies (PDF)

HPLC purity traces of compounds $\mathbf{1}^-$ to $\mathbf{9}^-$ and ^{11}B, ^{1}H, and ^{13}C NMR spectra of compounds $\mathbf{6}^-$ and $\mathbf{8}^-$ selected for detailed studies (PDF)

Molecular formula strings and some data for **1**−**9** (CSV)

Accession Codes

For crystal structures of $\mathbf{5}^-$ and $\mathbf{6}^-$ cocrystallized with a CAIX mimic−CAII enzyme, atomic coordinates and structure factors were deposited at the Worldwide Protein Data Bank under accession codes 5OGP and 5OGN. Authors will release the atomic coordinates upon article publication.

■ AUTHOR INFORMATION

Corresponding Authors

*B.G.: e-mail, gruner@iic.cas.cz; phone, +420 311236942.

*M.H.: e-mail, marian.hajduch@upol.cz; phone, +420 585632082.

*P.Ř.: e-mail, pavlina.rezacova@uochb.cas.cz; phone: +420 220 183 144.

ORCID

Bohumír Grüner: 0000-0002-2595-9125

Viswanath Das: 0000-0001-5973-5990

Jan Nekvinda: 0000-0001-8240-6271

Author Contributions

○B.G., J.B., V.D., V.Š., M.H., and P.Ř. contributed equally.

Notes

The authors declare the following competing financial interest(s): B.G., J.B., V.S., J.H., P.D., M.H., and P.R. are inventors of a United States Patent, Patent No. 9,290,529 B2, issued on March 22, 2016, that covers the title compounds.

■ ACKNOWLEDGMENTS

We thank Jaroslav Švehla (Institute of Inorganic Chemistry) and Dalibor Doležal (Institute of Molecular and Translation Medicine) for mass spectrometry and technical help with the animal experiments, respectively. This work was supported by the Czech Science Foundation, Projects 15-05677S and 18-27648S; the Technology Agency of the Czech Republic, Project TE01020028 (to M.H. and P.Ř.); and the Ministry of Education of the Czech Republic, Grants CZ.02.1.01/0.0/0.0/16_019/0000868 and EATRIS-CZ LM2015064. Support from Institutional Research Projects RVO 61388980, 68378050, and 61388963 of the Czech Academy of Sciences is also appreciated. We thank Czech-BioImaging for supporting the Raman imaging facility (Project LM2015062). Diffraction data have been collected on BL14 at the BESSY II electron storage ring operated by the Helmholtz-Zentrum Berlin.

■ ABBREVIATIONS USED

Caco-2, a continuous line of heterogeneous human epithelial colorectal adenocarcinoma cells; DMEM, Dulbecco's modified Eagle medium; DOX, doxorubicin; ESI, electrospray ionization; HEPES, 4-(2-hydroxyethyl)-1-piperazineethanesulfonic acid; MCS, multicellular spheroid; PAMPA, parallel artificial membrane permeability assay; PBS, phosphate buffered saline; RIPA, buffer solution used for lysis of cells

■ REFERENCES

(1) Cianchi, F.; Vinci, M. C.; Supuran, C. T.; Peruzzi, B.; De Giuli, P.; Fasolis, G.; Perigli, G.; Pastorekova, S.; Papucci, L.; Pini, A.; Masini, E.; Puccetti, L. Selective inhibition of carbonic anhydrase IX decreases cell proliferation and induces ceramide-mediated apoptosis in human cancer cells. *J. Pharmacol. Exp. Ther.* **2010**, *334*, 710−719.

(2) Ameis, H. M.; Drenckhan, A.; Freytag, M.; Izbicki, J. R.; Supuran, C. T.; Reinshagen, K.; Holland-Cunz, S.; Gros, S. J. Influence of hypoxia-dependent factors on the progression of neuroblastoma. *Pediatr. Surg. Int.* **2016**, *32*, 187−192.

(3) Lock, F. E.; McDonald, P. C.; Lou, Y. M.; Supuran, C. T.; Dedhar, S. The role of carbonic anhydrase IX in tumor hypoxia, metastasis and the cancer stem cell niche. *Cancer Res.* **2012**, *72*, 2−3.

(4) Neri, D.; Supuran, C. T. Interfering with pH regulation in tumours as a therapeutic strategy. *Nat. Rev. Drug Discovery* **2011**, *10*, 767−777.

(5) Chiche, J.; Ilc, K.; Laferriere, J.; Trottier, E.; Dayan, F.; Mazure, N. M.; Brahimi-Horn, M. C.; Pouyssegur, J. Hypoxia-inducible carbonic anhydrase IX and XII promote tumor cell growth by counteracting acidosis through the regulation of the intracellular pH. *Cancer Res.* **2009**, *69*, 358−368.

(6) McKenna, R.; Supuran, C. T. In *Carbonic Anhydrase: Mechanism, Regulation, Links to Disease, and Industrial Applications*; Frost, S. C., McKenna, R., Eds.; Springer: New York, 2014; Vol. *75*, pp 291−323.

(7) Aksu, K.; Nar, M.; Tanc, M.; Vullo, D.; Gulcin, I.; Goksu, S.; Tumer, F.; Supuran, C. T. Synthesis and carbonic anhydrase inhibitory properties of sulfamides structurally related to dopamine. *Bioorg. Med. Chem.* **2013**, *21*, 2925−2931.

(8) Bozdag, M.; Ferraroni, M.; Nuti, E.; Vullo, D.; Rossello, A.; Carta, F.; Scozzafava, A.; Supuran, C. T. Combining the tail and the ring approaches for obtaining potent and isoform-selective carbonic anhydrase inhibitors: Solution and X-ray crystallographic studies. *Bioorg. Med. Chem.* **2014**, *22*, 334−340.

(9) Winum, J. Y.; Supuran, C. T. Recent advances in the discovery of zinc-binding motifs for the development of carbonic anhydrase inhibitors. *J. Enzyme Inhib. Med. Chem.* **2015**, *30*, 321−324.

(10) Carta, F.; Supuran, C. T.; Scozzafava, A. Sulfonamides and their isosters as carbonic anhydrase inhibitors. *Future Med. Chem.* **2014**, *6*, 1149−1165.

(11) De Simone, G.; Alterio, V.; Supuran, C. T. Exploiting the hydrophobic and hydrophilic binding sites for designing carbonic anhydrase inhibitors. *Expert Opin. Drug Discovery* **2013**, *8*, 793−810.

(12) Supuran, C. T. How many carbonic anhydrase inhibition mechanisms exist? *J. Enzyme Inhib. Med. Chem.* **2016**, *31*, 345−360.

(13) Alterio, V.; Di Fiore, A.; D'Ambrosio, K.; Supuran, C. T.; De Simone, G. Multiple binding modes of inhibitors to carbonic anhydrases: How to design specific drugs targeting 15 different isoforms? *Chem. Rev.* **2012**, *112*, 4421−4468.

(14) Mikus, P.; Krajciova, D.; Mikulova, M.; Horvath, B.; Pecher, D.; Garaj, V.; Bua, S.; Angeli, A.; Supuran, C. T. Novel sulfonamides incorporating 1,3,5-triazine and amino acid structural motifs as inhibitors of the physiological carbonic anhydrase isozymes I, II and IV and tumor-associated isozyme IX. *Bioorg. Chem.* **2018**, *81*, 241−252.

DOI: 10.1021/acs.jmedchem.9b00945
J. Med. Chem. 2019, 62, 9560−9575

(15) Valliant, J. F.; Guenther, K. J.; King, A. S.; Morel, P.; Schaffer, P.; Sogbein, O. O.; Stephenson, K. A. The medicinal chemistry of carboranes. *Coord. Chem. Rev.* **2002**, *232*, 173−230.
(16) Scholz, M.; Hey-Hawkins, E. Carbaboranes as pharmacophores: Properties, synthesis, and application strategies. *Chem. Rev.* **2011**, *111*, 7035−7062.
(17) Issa, F.; Kassiou, M.; Rendina, M. Boron in drug discovery: Carboranes as uniquie pharmacophores in biologically active compounds. *Chem. Rev.* **2011**, *111*, 5701−5722.
(18) Grimes, R. N. *Carboranes*, 2nd ed.; Academic Press Publications: London, 2011.
(19) Satapathy, R.; Dash, B. P.; Maguire, J. A.; Hosmane, N. S. New developments in the medicinal chemistry of carboranes. *Collect. Czech. Chem. Commun.* **2010**, *75*, 995−1022.
(20) Lesnikowski, Z. J. Challenges and opportunities for the application of boron clusters in drug design. *J. Med. Chem.* **2016**, *59*, 7738−7758.
(21) Sibrian-Vazquez, M.; Hao, E.; Jensen, T. J.; Viccente, M. G. H. Enhanced cellular uptake with a cobaltacarborane−porphyrin−HIV-1 Tat 48−60 Conjugate. *Bioconjugate Chem.* **2006**, *17*, 928−934.
(22) Brynda, J.; Mader, P.; Šícha, V.; Fábry, M.; Poncová, K.; Bakardiev, M.; Grüner, B.; Cígler, P.; Řezáčová, P. Carborane-based carbonic anhydrase inhibitors. *Angew. Chem., Int. Ed.* **2013**, *52*, 13760−13763.
(23) Mader, P.; Pecina, A.; Cígler, P.; Lepšík, M.; Šícha, V.; Hobza, P.; Grüner, B.; Fanfrlík, J.; Brynda, J.; Řezáčová, P. Carborane-based carbonic anhydrase inhibitors: insight into CAII/CAIX specificity from a high-resolution crystal structure, modeling, and quantum chemical calculations. *BioMed Res. Int.* **2014**, *2014*, 389869.
(24) Hall, I. H.; Elkins, A.; Powell, W. J.; Karthikeyan, S.; Sood, A.; Spielvogel, B. F. Substituted carboranes and polyhedral hydroborate salts as anti-neoplastics. *Anticancer Res.* **1998**, *18*, 2617−2622.
(25) Gabel, D. Boron clusters in medicinal chemistry: perspectives and problems. *Pure Appl. Chem.* **2015**, *87*, 173−179.
(26) Hall, I. H.; Warren, A. E.; Lee, C. C.; Wasczcak, M. D.; Sneddon, L. G. Cytotoxicity of ferratricarbadecaboranyl complexes in murine and human tissue cultured cell lines. *Anticancer Res.* **1998**, *18*, 951−962.
(27) Hall, I. H.; Lackey, C. B.; Kistler, T. D.; Durham, R. W.; Russell, J. M.; Grimes, R. N. Antitumor activity of mono- and dimetallic transition metal carborane complexes of Ta, Fe, Co, Mo, or W. *Anticancer Res.* **2000**, *20*, 2345−2354.
(28) Hall, I. H.; Tolmie, C. E.; Barnes, B. J.; Curtis, M. A.; Russell, J. M.; Finn, M. G.; Grimes, R. N. Cytotoxicity of tantalum(V) and niobium(V) small carborane complexes and mode of action in P388 lymphocytic leukemia cells. *Appl. Organomet. Chem.* **2000**, *14*, 108−118.
(29) Cígler, P.; Kožíšek, M.; Řezáčová, P.; Brynda, J.; Otwinowski, Z.; Pokorná, J.; Plešek, J.; Grüner, B.; Doležková-Marešová, L.; Máša, M.; Sedláček, J.; Bodem, J.; Krausslich, H. G.; Král, V.; Konvalinka, J. From nonpeptide toward noncarbon protease inhibitors: Metallacarboranes as specific and potent inhibitors of HIV protease. *Proc. Natl. Acad. Sci. U. S. A.* **2005**, *102*, 15394−15399.
(30) Kožíšek, M.; Cígler, P.; Lepšík, M.; Fanfrlík, J.; Řezáčová, P.; Brynda, J.; Pokorná, J.; Plešek, J.; Grüner, B.; Grantz-Šašková, K.; Václavíková, J.; Kraeusslich, H. G.; Král, V.; Konvalinka, J. Inorganic polyhedral metallacarborane inhibitors of HIV protease: a new approach to overcoming antiviral resistance. *J. Med. Chem.* **2008**, *51*, 4839−4843.
(31) Řezáčová, P.; Pokorná, J.; Brynda, J.; Kožíšek, M.; Cígler, P.; Lepšík, M.; Fanfrlík, J.; Řezáč, J.; Šašková, K. G.; Sieglová, I.; Plešek, J.; Šícha, V.; Grüner, B.; Oberwinkler, H.; Sedláček, J.; Kraeusslich, H. G.; Hobza, P.; Král, V.; Konvalinka, J. Design of HIV protease inhibitors based on inorganic polyhedral metallacarboranes. *J. Med. Chem.* **2009**, *52*, 7132−7141.
(32) Řezáčová, P.; Cígler, P.; Matějíček, P.; Pokorná, J.; Grüner, B.; Konvalinka, J. Medicinal Application of Carboranes Inhibition of HIV Protease. In *Boron Science: New Technologies and Applications*; CRC Press Taylor and Francis Group: Boca Raton, FL, 2012; pp 41−70.
(33) Ilinova, A.; Semioshkin, A.; Lobanova, I.; Bregadze, V. I.; Mironov, A. F.; Paradowska, E.; Studzinska, M.; Jablonska, A.; Bialek-Pietras, M.; Lesnikowski, Z. J. Synthesis, cytotoxicity and antiviral activity studies of the conjugates of cobalt bis(1,2-dicarbollide)(-I) with 5-ethynyl-2′-deoxyuridine and its cyclic derivatives. *Tetrahedron* **2014**, *70*, 5704−5710.
(34) Verdia-Baguena, C.; Alcaraz, A.; Aguilella, V. M.; Cioran, A. M.; Tachikawa, S.; Nakamura, H.; Teixidor, F.; Viñas, C. Amphiphilic COSAN and I2-COSAN crossing synthetic lipid membranes: planar bilayers and liposomes. *Chem. Commun.* **2014**, *50*, 6700−6703.
(35) Popova, T.; Zaulet, A.; Teixidor, F.; Alexandrova, R.; Viñas, C. Investigations on antimicrobial activity of cobaltabisdicarbollides. *J. Organomet. Chem.* **2013**, *747*, 229−234.
(36) Kvasničková, E.; Masák, J.; Čejka, J.; Maťátková, O.; Šícha, V. Preparation, characterization, and the selective antimicrobial activity of N-alkylammonium 8-diethyleneglycol cobalt bis-dicarbollide derivatives. *J. Organomet. Chem.* **2017**, *827*, 23−31.
(37) De Simone, G.; Supuran, C. T. (In)organic anions as carbonic anhydrase inhibitors. *J. Inorg. Biochem.* **2012**, *111*, 117−129.
(38) Plešek, J.; Heřmánek, S.; Franken, A.; Císařová, I.; Nachtigal, C. Dimethyl sulfate induced nucleophilic substitution of the bis(1,2-dicarbollido)-3-cobalt(1-) ate ion. Syntheses, properties and structures of its 8,8′-mu-sulfato, 8-phenyl and 8-dioxane derivatives. *Collect. Czech. Chem. Commun.* **1997**, *62*, 47−56.
(39) Llop, J.; Masalles, C.; Viñas, C.; Teixidor, F.; Sillanpää, R.; Kivekäs, R. The [3,3 '-Co(1,2-C2B9H11)(2)](-) anion as a platform for new materials: synthesis of its functionalized monosubstituted derivatives incorporating synthons for conducting organic polymers. *Dalton Trans* **2003**, 556−561.
(40) Semioshkin, A. A.; Sivaev, I. B.; Bregadze, V. I. Cyclic oxonium derivatives of polyhedral boron hydrides and their synthetic applications. *Dalton Trans* **2008**, *2008*, 977−992.
(41) Plešek, J.; Grüner, B.; Šícha, V.; Böhmer, V.; Císařová, I. The zwitterion (8,8 '-μ-CH2O(CH3)-(1,2-C2B9H10)2-3,3′-Co (0) as a versatile building block to introduce cobalt bis(dicarbollide) ion into organic molecules. *Organometallics* **2012**, *31*, 1703−1715.
(42) Grüner, B.; Švec, P.; Šícha, V.; Padělková, Z. Direct and facile synthesis of carbon substituted alkylhydroxy derivatives of cobalt bis(1,2-dicarbollide), versatile building blocks for synthetic purposes. *Dalton Trans* **2012**, *41*, 7498−7512.
(43) Nekvinda, J.; Švehla, J.; Císařová, I.; Grüner, B. Chemistry of cobalt bis(1,2-dicarbollide) ion; the synthesis of carbon substituted alkylamino derivatives from hydroxyalkyl derivatives via methylsulfonyl or p-toluenesulfonyl esters. *J. Organomet. Chem.* **2015**, *798*, 112−120.
(44) Chamberlin, R. M.; Scott, B. L.; Melo, M. M.; Abney, K. D. Butyllithium deprotonation vs alkali metal reduction of cobalt dicarbollide: A new synthetic route to C-substituted derivatives. *Inorg. Chem.* **1997**, *36*, 809−817.
(45) Olejniczak, A. B.; Milecki, J.; Schroeder, G. The effect of stereochemistry on sodium ion complexation in nucleoside-metallacarborane conjugates. *Bioinorg. Chem. Appl.* **2010**, *2019*, 196064.
(46) Tarrés, M.; Viñas, C.; Gonzalez-Cardoso, P.; Hanninen, M. M.; Sillanpaa, R.; Dordovic, V.; Uchman, M.; Teixidor, F.; Matějíček, P. Aqueous self-assembly and cation selectivity of cobaltabisdicarbollide dianionic dumbbells. *Chem. - Eur. J.* **2014**, *20*, 6786−6794.
(47) Plešek, J.; Grüner, B.; Heřmánek, S.; Báča, J.; Mareček, V.; Jänchenová, J.; Lhotský, A.; Holub, K.; Selucký, P.; Rais, J.; Císařová, I.; Čáslavský, J. Synthesis of functionalized cobaltacarboranes based on the closo- (1,2-C2B9H11)(2)-3,3 '-Co (−) ion bearing polydentate ligands for separation of M3+ cations from nuclear waste solutions. Electrochemical and liquid-liquid extraction study of selective transfer of M3+ metal cations to an organic phase. Molecular structure of the closo- (8-(2-CH3O-C5H4-O)- (CH2CH2O)(2)-1,2-C2B9H10)-(1 ',2'-C2B9H11)-3,3'-Co Na determined by X-ray diffraction analysis. *Polyhedron* **2002**, *21*, 975−986.
(48) Matějíček, P.; Cígler, P.; Procházka, K.; Král, V. Molecular assembly of metallacarboranes in water: Light scattering and microscopy study. *Langmuir* **2006**, *22*, 575−581.

DOI: 10.1021/acs.jmedchem.9b00945
J. Med. Chem. 2019, 62, 9560−9575

(49) Dordovic, V.; Tošner, Z.; Uchman, M.; Zhigunov, A.; Reza, M.; Ruokolainen, J.; Pramanik, G.; Cígler, P.; Kalikova, K.; Gradzielski, M.; Matějícek, P. Stealth amphiphiles: Self-assembly of polyhedral boron clusters. *Langmuir* **2016**, *32*, 6713−6722.
(50) Uchman, M.; Dordovic, V.; Tošner, Z.; Matějíček, P. Classical amphiphilic behavior of nonclassical amphiphiles: A comparison of metallacarborane self-assembly with SDS micellization. *Angew. Chem., Int. Ed.* **2015**, *54*, 14113−14117.
(51) Pinard, M. A.; Boone, C. D.; Rife, B. D.; Supuran, C. T.; McKenna, R. Structural study of interaction between brinzolamide and dorzolamide inhibition of human carbonic anhydrases. *Bioorg. Med. Chem.* **2013**, *21*, 7210−7215.
(52) Mujumdar, P.; Teruya, K.; Tonissen, K. F.; Vullo, D.; Supuran, C. T.; Peat, T. S.; Poulsen, S. A. An unusual natural product primary sulfonamide: Synthesis, carbonic anhydrase inhibition, and protein X-ray structures of Psammaplin C. *J. Med. Chem.* **2016**, *59*, 5462−5470.
(53) Winum, J. Y.; Scozzafava, A.; Montero, J. L.; Supuran, C. T. Therapeutic potential of sulfamides as enzyme inhibitors. *Med. Res. Rev.* **2006**, *26*, 767−792.
(54) De Simone, G.; Langella, E.; Esposito, D.; Supuran, C. T.; Monti, S. M.; Winum, J. Y.; Alterio, V. Insights into the binding mode of sulphamates and sulphamides to hCA II: crystallographic studies and binding free energy calculations. *J. Enzyme Inhib. Med. Chem.* **2017**, *32*, 1002−1011.
(55) Di Fiore, A.; Monti, S. M.; Innocenti, A.; Winum, J.-Y.; De Simone, G.; Supuran, C. T. Carbonic anhydrase inhibitors: Crystallographic and solution binding studies for the interaction of a boron-containing aromatic sulfamide with mammalian isoforms I-XV. *Bioorg. Med. Chem. Lett.* **2010**, *20*, 3601−3605.
(56) Lou, Y. M.; McDonald, P. C.; Oloumi, A.; Chia, S.; Ostlund, C.; Ahmadi, A.; Kyle, A.; auf dem Keller, U.; Leung, S.; Huntsman, D.; Clarke, B.; Sutherland, B. W.; Waterhouse, D.; Bally, M.; Roskelley, C.; Overall, C. M.; Minchinton, A.; Pacchiano, F.; Carta, F.; Scozzafava, A.; Touisni, N.; Winum, J. Y.; Supuran, C. T.; Dedhar, S. Targeting tumor hypoxia: Suppression of breast tumor growth and metastasis by novel carbonic anhydrase IX inhibitors. *Cancer Res.* **2011**, *71*, 3364−3376.
(57) McIntyre, A.; Patiar, S.; Wigfield, S.; Li, J. L.; Ledaki, I.; Turley, H.; Leek, R.; Snell, C.; Gatter, K.; Sly, W. S.; Vaughan-Jones, R. D.; Swietach, P.; Harris, A. L. Carbonic anhydrase IX promotes tumor growth and necrosis in vivo and inhibition enhances anti-VEGF therapy. *Clin. Cancer Res.* **2012**, *18*, 3100−3111.
(58) Yang, J. S.; Lin, C. W.; Hsieh, Y. H.; Chien, M. H.; Chuang, C. Y.; Yang, S. F. Overexpression of carbonic anhydrase IX induces cell motility by activating matrix metalloproteinase-9 in human oral squamous cell carcinoma cells. *Oncotarget* **2017**, *8*, 83088−83099.
(59) Ji, T. J.; Lang, J. Y.; Wang, J.; Cai, R.; Zhang, Y. L.; Qi, F. F.; Zhang, L. J.; Zhao, X.; Wu, W. J.; Hao, J. H.; Qin, Z. H.; Zhao, Y.; Nie, G. J. Designing liposomes to suppress extracellular matrix expression to enhance drug penetration and pancreatic tumor therapy. *ACS Nano* **2017**, *11*, 8668−8678.
(60) Salmon, A. J.; Williams, M. L.; Wu, Q. K.; Morizzi, J.; Gregg, D.; Charman, S. A.; Vullo, D.; Supuran, C. T.; Poulsen, S. A. Metallocene-based inhibitors of cancer-associated carbonic anhydrase enzymes IX and XII. *J. Med. Chem.* **2012**, *55*, 5506−5517.
(61) Grüner, B.; Plzák, Z. High-performance liquid chromatographic separations of boron-cluster compounds. *J. Chromatogr. A* **1997**, *789*, 497−517.
(62) Nekvinda, J.; Šícha, V.; Hnyk, D.; Grüner, B. Synthesis, characterisation and some chemistry of C- and B-substituted carboxylic acids of cobalt bis(dicarbollide). *Dalton Trans* **2014**, *43*, 5106−5120.
(63) Sivaev, I. B.; Starikova, Z. A.; Sjoberg, S.; Bregadze, V. I. Synthesis of functional derivatives of the 3,3′-Co(1,2- C2B2H11)(2) (-) anion. *J. Organomet. Chem.* **2002**, *649*, 1−8.
(64) Müller, U.; Darowski, N.; Fuchs, M. R.; Forster, R.; Hellmig, M.; Paithankar, K. S.; Puhringer, S.; Steffien, M.; Zocher, G.; Weiss, M. S. Facilities for macromolecular crystallography at the Helmholtz-Zentrum Berlin. *J. Synchrotron Radiat.* **2012**, *19*, 442−449.
(65) Kabsch, W. Integration, scaling, space-group assignment and post-refinement. *Acta Crystallogr., Sect. D: Biol. Crystallogr.* **2010**, *66*, 133−144.
(66) Kabsch, W. XDS. *Acta Crystallogr., Sect. D: Biol. Crystallogr.* **2010**, *66*, 125−132.
(67) Mader, P.; Brynda, J.; Gitto, R.; Agnello, S.; Pachl, P.; Supuran, C. T.; Chimirri, A.; Řezáčová, P. Structural basis for the interaction between carbonic anhydrase and 1,2,3,4-tetrahydroisoquinolin-2-ylsulfonamides. *J. Med. Chem.* **2011**, *54*, 2522−2526.
(68) Ditte, P.; Dequiedt, F.; Svastova, E.; Hulikova, A.; Ohradanova-Repic, A.; Zatovicova, M.; Csaderova, L.; Kopáček, J.; Supuran, C. T.; Pastorekova, S.; Pastorek, J. Phosphorylation of carbonic anhydrase IX controls its ability to mediate extracellular acidification in hypoxic tumors. *Cancer Res.* **2011**, *71*, 7558−7567.
(69) Xu, Y. Z.; Heravi, M.; Thuraisingam, T.; Di Marco, S.; Muanza, T.; Radzioch, D. Brg-1 mediates the constitutive and fenretinide-induced expression of SPARC in mammary carcinoma cells via its interaction with transcription factor Sp1. *Mol. Cancer* **2010**, *9*, 210.
(70) Nosková, V.; Džubák, P.; Kuzmina, G.; Ludková, A.; Stehlik, D.; Trojanec, R.; Janostáková, A.; Kořínková, G.; Mihal, V.; Hajdúch, M. In vitro chemoresistance profile and expression/function of MDR associated proteins in resistant cell lines derived from CCRF-CEM, K562, A549 and MDA MB 231 parental cells. *Neoplasma* **2002**, *49*, 418−425.
(71) Das, V.; Furst, T.; Gurská, S.; Džubák, P.; Hajdúch, M. Evaporation-reducing culture condition increases the reproducibility of multicellular spheroid formation in microtiter plates. *J. Visualized Exp.* **2017**, No. 121, e55403.
(72) Weiswald, L. B.; Guinebretiere, J. M.; Richon, S.; Bellet, D.; Saubamea, B.; Dangles-Marie, V. In situ protein expression in tumour spheres: development of an immunostaining protocol for confocal microscopy. *BMC Cancer* **2010**, *10*, 11.
(73) Pampaloni, F.; Richa, R.; Ansari, N.; Stelzer, E. H. Live spheroid formation recorded with light sheet-based fluorescence microscopy. *Methods Mol. Biol.* **2015**, *1251*, 43−57.
(74) Gong, M. Q.; Wu, J. L.; Chen, B.; Zhuo, R. X.; Cheng, S. X. Self-assembled polymer/ inorganic hybrid nanovesicles for multiple drug delivery to overcome drug resistance in cancer chemotherapy. *Langmuir* **2015**, *31*, 5115−5122.
(75) Perlíková, P.; Rylová, G.; Naus, P.; Elbert, T.; Tloušťová, E.; Bourderioux, A.; Slavětínská, L. P.; Motyka, K.; Doležal, D.; Znojek, P.; Nová, A.; Harvanová, M.; Džubák, P.; Siller, M.; Hlaváč, J.; Hajdúch, M.; Hocek, M. 7-(2-Thienyl)-7-deazaadenosine (AB61), a new potent nucleoside cytostatic with a complex mode of action. *Mol. Cancer Ther.* **2016**, *15*, 922−937.
(76) Williams, J. W.; Morrison, J. F. The kinetics of reversible tight-binding inhibition. In *Enzyme Kinetics and Mechanism Part A Initial Rate and Inhibitor Methods*; Methods in Enzymology Series; Elsevier: Amsterdam, Netherlands, 1979; Vol. *63*; pp 437−467.

NOTE ADDED IN PROOF

Reference 76 was added to the text at the proof stage.

DOI: 10.1021/acs.jmedchem.9b00945
J. Med. Chem. 2019, 62, 9560−9575